Bilinear R Parity Violating Supersymmetry searches at $\sqrt{s} = 7$ TeV and $L = 35\,\text{pb}^{-1}$ with the ATLAS Detector

Fernando Quiñónez

Pontificia Universidad Católica de Chile

2011-07-21

Table of contents

Equations 1 and 2 represent the BRPV susy superpotential and the soft lagrangian respectively, and describes the model under consideration throught this thesis,

$$W_{\text{BRPV}} = W_{\text{MSSM}} + V_{\text{BRPV}}, \tag{1}$$

$$\mathcal{L}^{\text{BRPV}}_{\text{soft}} = \mathcal{L}^{\text{soft}}_{\text{MSSM}} + \mathcal{V}^{\text{soft}}_{\text{BRPV}}. \tag{2}$$

Eq. 3 is the superpotential of the MSSM

$$W_{\text{MSSM}} = \varepsilon_{ab}\left[h^{ij}_U \widehat{Q}^a_i \widehat{U}_j \widehat{H}^b_u + h^{ij}_D \widehat{Q}^b_i \widehat{D}_j \widehat{H}^a_d + h^{ij}_E \widehat{L}^b_i \widehat{R}_j \widehat{H}^a_d - \mu \widehat{H}^a_d \widehat{H}^b_u\right], \tag{3}$$

with ε_{ab} the Levy-Civita symbol for two dimensions, h_U, h_D, and h_E are the Yukawa matrices. And μ is the supersymmetric Higgs mass parameter. Equation 4 is the term responsible for the bilinear R parity violation.

$$V_{\text{BRPV}} = \varepsilon_{ab}\epsilon_i \widehat{L}^a_i \widehat{H}^b_u \tag{4}$$

This is said to be bilinear because it is the product of two superfields. The bilinear R parity violating couplings ϵ_i are introduced, and are free parameters of the theory. With the introduction of BRPV, the model lost the Neutralino $\tilde{\chi}^0_1$ as candidate for dark matter (since $\tilde{\chi}^0_1$ decays, a feature that differs of R Parity Conserving RPC models). Following a mechanism that will be described soon, this model gives masses to the neutrinos.

The second most important function is the density lagrangian that includes the soft terms. The soft terms are contribution on the masses of all the superpartners that evindently do not have the same mass of the standard model particles, which is

$$\begin{aligned}
\mathcal{L}^{\text{soft}}_{\text{MSSM}} &= M_Q^{ij2}\widetilde{Q}_i^{a*}\widetilde{Q}_j^a + M_U^{ij2}\widetilde{U}_i\widetilde{U}_j^* + M_D^{ij2}\widetilde{D}_i\widetilde{D}_j^* \\
&+ M_L^{ij2}\widetilde{L}_i^{a*}\widetilde{L}_j^a + M_R^{ij2}\widetilde{R}_i\widetilde{R}_j^* \\
&+ m_{H_d}^2 H_d^{a*} H_d^a + m_{H_u}^2 H_u^{a*} H_u^a \\
&- \left[\frac{1}{2}M_3\lambda_s\lambda_s + \frac{1}{2}M_2\lambda\lambda + \frac{1}{2}M_1\lambda'\lambda' + h.c.\right] \\
&+ \varepsilon_{ab}\left[A_U^{ij}\widetilde{Q}_i^a\widetilde{U}_j H_u^b + A_D^{ij}\widetilde{Q}_i^b\widetilde{D}_j H_d^a + A_E^{ij}\widetilde{L}_i^b\widetilde{R}_j H_d^a - B\mu H_d^a H_u^b\right]
\end{aligned} \tag{5}$$

and of course, the BRPV term in the superpotential has a corresponding soft BRPV term

$$\mathcal{V}^{soft}_{BRPV} = -B_i\epsilon_i\varepsilon_{ab}\widetilde{L}_i^a H_u^b. \tag{6}$$

The soft lagrangian is responsible for the explicit supersymmetry breaking.

R-Parity

The R-Parity is defined by:

$$R_p = (-1)^{3B+2S+L} = \begin{cases} +1 \text{ for SM particles} \\ -1 \text{ for superpartners,} \end{cases} \tag{7}$$

with B the barionic number, S the spin, and L the leptonic number.

BRPV scalar content

The scalars content of the BRPV susy model is the same as the MSSM, however in this model the sneutrinos acquire vacuum expectation values. The fields are:

$$H_d = \begin{pmatrix} H_d^0 \\ H_d^- \end{pmatrix}, \qquad H_u = \begin{pmatrix} H_u^+ \\ H_u^0 \end{pmatrix}, \qquad \widetilde{L}_i = \begin{pmatrix} \tilde{L}_i^0 \\ \tilde{\ell}_i^- \end{pmatrix}, \tag{8}$$

and when they break the electroweak symmetry spontaneously, become:

$$H_d^0 \equiv \frac{1}{\sqrt{2}}[\sigma_d^0 + v_d + i\varphi_d^0], \quad H_u^0 \equiv \frac{1}{\sqrt{2}}[\sigma_u^0 + v_u + i\varphi_u^0], \quad \tilde{L}_i^0 \equiv \frac{1}{\sqrt{2}}[\tilde{\nu}_i^R + v_i + i\tilde{\nu}_i^I], \tag{9}$$

with v_i, $i = 1, 2, 3$ are the sneutrino vevs, and v_u, v_d are the usual Higgs vevs of the MSSM. The vacuum expectation values satisfy

$$v^2 \equiv v_d^2 + v_u^2 + v_1^2 + v_2^2 + v_3^2 \tag{10}$$

and the W boson acquires mass $m_W = gv/2$, with $v = 246$ GeV. The MSSM is recovered by making $v_i = \epsilon_i = 0$. Since v_1, v_2, $v_3 \ll v_u$, v_d the relation $\tan\beta = v_u/v_d$ is keeped. With respect to the free parameters of this model, they are the same as the MSSM plus v_i and either the set of ϵ_i, or the set of B_i, but not both sets because one can be solved in function of the other as is described in *Neutrino masses and mixings from supersymmetry with billinear R-parity violation: A theory for solar and atmospheric neutrino oscillations. hep-ph0004115v2*

Neutral Fermions

The neutral fermions of this model are: two gauginos, two higgsinos and three neutrinos, so in the basis

$$\psi^{0T} = (-i\lambda', -i\lambda^3, \widetilde{H}_d^1, \widetilde{H}_u^2, \nu_e, \nu_\mu, \nu_\tau) \tag{11}$$

the neutral fermion mass matrix M_N is given by

$$M_N = \begin{pmatrix} \mathcal{M}_{\chi^0} & m^T \\ m & 0 \end{pmatrix}, \tag{12}$$

where

$$\mathcal{M}_{\chi^0} = \begin{pmatrix} M_1 & 0 & -\frac{1}{2}g' v_d & \frac{1}{2}g' v_u \\ 0 & M_2 & \frac{1}{2}g v_d & -\frac{1}{2}g v_u \\ -\frac{1}{2}g' v_d & \frac{1}{2}g v_d & 0 & -\mu \\ \frac{1}{2}g' v_u & -\frac{1}{2}g v_u & -\mu & 0 \end{pmatrix} \tag{13}$$

is the standard MSSM neutralino mass matrix and

$$m = \begin{pmatrix} -\frac{1}{2}g' v_1 & \frac{1}{2}g v_1 & 0 & \epsilon_1 \\ -\frac{1}{2}g' v_2 & \frac{1}{2}g v_2 & 0 & \epsilon_2 \\ -\frac{1}{2}g' v_3 & \frac{1}{2}g v_3 & 0 & \epsilon_3 \end{pmatrix} \tag{14}$$

characterizes the breaking of R-parity. The mass matrix M_N in eq. 12 is block diagonalized by $\mathcal{N}_F$

$$\mathcal{N}_F^* M_N \mathcal{N}_F^{-1} = \begin{pmatrix} \mathcal{M}_{\chi^0} & 0_{4\times 3} \\ 0_{3\times 4} & m_{\text{eff}} \end{pmatrix} = M_{NB} \tag{15}$$

with

$$m_{\text{eff}} = -m \cdot \mathcal{M}_{\chi^0}^{-1} m^T = \frac{M_1 g^2 + M_2 g'^2}{4 \det(\mathcal{M}_{\chi^0})} \begin{pmatrix} \Lambda_e^2 & \Lambda_e\Lambda_\mu & \Lambda_e\Lambda_\tau \\ \Lambda_e\Lambda_\mu & \Lambda_\mu^2 & \Lambda_\mu\Lambda_\tau \\ \Lambda_e\Lambda_\tau & \Lambda_\mu\Lambda_\tau & \Lambda_\tau^2 \end{pmatrix}, \tag{16}$$

with

$$\Lambda_i = \mu v_i + v_d \epsilon_i \tag{17}$$

are the alignment parameters.

The block-diagonalizing matrix can be written as,

$$\mathcal{N}_F^* = \begin{pmatrix} 1 - \frac{1}{2}\xi^\dagger\xi & \xi^\dagger \\ -\xi & 1 - \frac{1}{2}\xi\xi^\dagger \end{pmatrix}, \tag{18}$$

with,

$$\xi = m \cdot \mathcal{M}_{\chi^0}^{-1}, \qquad \forall \xi_{ij} \ll 1, \tag{19}$$

where $(j = 1, \cdots, 4)$ for the neutralinos, and $(i = 1, \cdots, 3)$ for the neutrinos. Explicitly

$$\xi_{i1} = \frac{g' M_2 \mu}{2 \det(\mathcal{M}_{\chi^0})} \Lambda_i \tag{20}$$

$$\xi_{i2} = -\frac{g M_1 \mu}{2 \det(\mathcal{M}_{\chi^0})} \Lambda_i \tag{21}$$

$$\xi_{i3} = -\frac{\epsilon_i}{\mu} + \frac{(g^2 M_1 + g'^2 M_2) v_u}{4 \det(\mathcal{M}_{\chi^0})} \Lambda_i \tag{22}$$

$$\xi_{i4} = -\frac{(g^2 M_1 + g'^2 M_2) v_d}{4 \det(\mathcal{M}_{\chi^0})} \Lambda_i \tag{23}$$

From the last equations and 17 one can see that $\xi = 0$ in the MSSM limit where $\epsilon_i = 0$, $v_i = 0$.

The matrix that diagonalize 15 is:

$$\mathcal{N}_L^* = \mathcal{N}_T^* \cdot \mathcal{N}_S^* = \begin{pmatrix} 1 & 0 \\ 0 & V_\nu^T \end{pmatrix} \times \begin{pmatrix} N^* & 0 \\ 0 & 1 \end{pmatrix}, \tag{24}$$

the sub-matrices N and V_ν diagonalize $\mathcal{M}_{\chi^0}$ and m_{eff}.

$$N^* \mathcal{M}_{\chi^0} N^\dagger = \text{diag}(m_{\chi_1^0}, m_{\chi_2^0}, m_{\chi_3^0}, m_{\chi_4^0}), \tag{25}$$

$$V_\nu^T m_{\text{eff}} V_\nu = \text{diag}(0, 0, m_\nu), \tag{26}$$

where

$$m_\nu = \text{Tr}(m_{\text{eff}}) = \frac{M_1 g^2 + M_2 g'^2}{4 \det(\mathcal{M}_{\chi^0})} |\vec{\Lambda}|^2. \tag{27}$$

As is seen, only one neutrino acquires mass, this is a feature often encountered in R parity violating models.

As a result one of the three angles in the matrix V_ν is undetermined, leading to

$$V_\nu = \begin{pmatrix} 1 & 0 & 0 \\ 0 & \cos\theta_{23} & -\sin\theta_{23} \\ 0 & \sin\theta_{23} & \cos\theta_{23} \end{pmatrix} \times \begin{pmatrix} \cos\theta_{13} & 0 & -\sin\theta_{13} \\ 0 & 1 & 0 \\ \sin\theta_{13} & 0 & \cos\theta_{13} \end{pmatrix}, \tag{28}$$

where the mixing angles can be expressed in terms of the components of the *alignment vector* $\vec{\Lambda}$ as follows and are related with the neutrino experiement angles as:

$$\tan\theta_{\text{sol}} \equiv \tan\theta_{13} = -\frac{\Lambda_e}{\sqrt{\Lambda_\mu^2 + \Lambda_\tau^2}}, \tag{29}$$

$$\tan\theta_{\text{atm}} \equiv \tan\theta_{23} = \frac{\Lambda_\mu}{\Lambda_\tau}. \tag{30}$$

A second neutrino acquires mass if the one-loop contributions are taken into account, the interested may read *Neutrino masses and mixings from supersymmetry with billinear R-parity violation: A theory for solar and atmospheric neutrino oscillations. hep-ph0004115v2*.

Charged Fermions

The charginos mix with the charged leptons to form a set of five charged fermions $F_i^{\pm}$, $i = 1, \ldots, 5$. In the basis

$$\psi^{+T} = (-i\lambda^+, \widetilde{H}_u^+, e_R^+, \mu_R^+, \tau_R^+), \text{ and } \quad \psi^{-T} = (-i\lambda^-, \widetilde{H}_d^-, e_L^-, \mu_L^-, \tau_L^-), \tag{31}$$

the charged fermion mass terms in the Lagrangian are

$$\mathcal{L}_m = -\frac{1}{2}(\psi^{-T} M_C \psi^+ + \psi^{+T} M_C^T \psi^-) + h.c. \tag{32}$$

where the chargino/lepton mass matrix is given by

$$M_C = \begin{pmatrix} \Delta_+ & \Delta_{12} \\ \Delta_{21} & \Delta_l \end{pmatrix} \tag{33}$$

with

$$\Delta_+ = \begin{pmatrix} M_2 & \frac{1}{\sqrt{2}} g v_u \\ \frac{1}{\sqrt{2}} g v_d & \mu \end{pmatrix}, \tag{34}$$

$$\Delta_{12} = \begin{pmatrix} 0 & 0 & 0 \\ -\frac{1}{\sqrt{2}} (h_E)_{11} v_1 & -\frac{1}{\sqrt{2}} (h_E)_{22} v_2 & -\frac{1}{\sqrt{2}} (h_E)_{33} v_3 \end{pmatrix}, \tag{35}$$

$$\Delta_{21} = \begin{pmatrix} \frac{1}{\sqrt{2}} g v_1 & -\epsilon_1 \\ \frac{1}{\sqrt{2}} g v_2 & -\epsilon_2 \\ \frac{1}{\sqrt{2}} g v_3 & -\epsilon_3 \end{pmatrix}, \tag{36}$$

$$\Delta_l = \begin{pmatrix} \frac{1}{\sqrt{2}} (h_E)_{11} v_d & 0 & 0 \\ 0 & \frac{1}{\sqrt{2}} (h_E)_{22} v_d & 0 \\ 0 & 0 & \frac{1}{\sqrt{2}} (h_E)_{33} v_d \end{pmatrix}, \tag{37}$$

with M_2 the $SU(2)$ gaugino soft mass.

Also the chargino sector decouples from the lepton sector in the limit $\epsilon_i = v_i = 0$. As in the MSSM, the chargino mass matrix is diagonalized by two rotation matrices $\mathcal{U}$ and $\mathcal{V}$ defined by

$$\mathcal{U}^* M_C \mathcal{V}^{-1} = M_{CD}, \tag{38}$$

where M_{CD} is the diagonal charged fermion mass matrix. To determine $\mathcal{U}$ and $\mathcal{V}$ we note that

$$M_{CD}^2 = \mathcal{V} M_C^\dagger M_C \mathcal{V}^{-1} = \mathcal{U}^* M_C M_C^\dagger (\mathcal{U}^*)^{-1} \tag{39}$$

implying that $\mathcal{V}$ diagonalizes $M_C^\dagger M_C$ and $\mathcal{U}^*$ diagonalizes $M_C M_C^\dagger$. For future reference we note that

$$\psi_j^- = \mathcal{U}_{kj}^* F_k^- \quad ; \quad \psi_j^+ = \mathcal{V}_{kj}^* F_k^+ \tag{40}$$

where $F_i^\pm$ are the chargino mass eigenstates in Weyl basis

$$F_i^- = \mathcal{U}_{ij} \psi_j^- \quad ; \quad F_i^+ = \mathcal{V}_{ij} \psi_j^+. \tag{41}$$

In the previous expressions the $F_i^\pm$ are two component spinors.

The four component Dirac spinors are constructed out of the two component spinors with the conventions

$$\tilde{\chi}_i^- = \begin{pmatrix} F_i^- \\ \overline{F_i^+} \end{pmatrix}. \tag{42}$$

The following approximations will be useful in the next section. If we take the eq. 18 to be

$$\mathcal{N}_F^* = \begin{pmatrix} 1 & \xi^\dagger \\ -\xi & 1 \end{pmatrix}, \tag{43}$$

then the matrix $\mathcal{N}^*$ is

$$\mathcal{N}^* = \mathcal{N}_L^* \cdot \mathcal{N}_F^* = \begin{pmatrix} N^* & N^* \xi^\dagger \\ -V_\nu^T \xi & V_\nu^T \end{pmatrix}. \tag{44}$$

Charged fermions block diagonalization and approximations

An analogous procedure to the block diagonalization on the neutralinos mass matrix can be done with the charginos mass matrix, and also an approximation on the diagonalizing matrices $\mathcal{U}$ and $\mathcal{V}$,
as seen in *Supersymmetric origin of neutrino mass. New. J. Phys., (76), 2004.*

$$\mathcal{V} = \begin{pmatrix} V & V\xi_R^T \\ -V_R^I \xi_R^* & V_R^I \end{pmatrix}, \tag{45}$$

and

$$\mathcal{U} = \begin{pmatrix} U & U\xi_L^\dagger \\ -V_L^{I*}\xi_L & V_L^{I*} \end{pmatrix} \tag{46}$$

with

$$\xi_{L\,i1} = \frac{g}{\sqrt{2}\det(\Delta_+)}\Lambda_i, \qquad \xi_{L\,i2} = -\frac{g^2 v_u}{2\mu\det(\Delta_+)}\Lambda_i - \frac{\epsilon_i}{\mu}, \tag{47}$$

$$\xi_R \approx \frac{m_l}{m_{susy}} \approx 0_{2\times 3}, \tag{48}$$

m_{susy} is the susy mass scale and $m_{susy} \approx (M_2, \mu)$.

The $\tilde{\chi}_1^0 \to \mu jj$ Channel

The neutralino lagrangian in Dirac spinors is given by

$$\begin{aligned}
\mathcal{L}_{\text{neutralino}} &= \overline{\chi_i^-}(O_{L\,ij}^{cns} P_L + O_{R\,ij}^{cns} P_R)\chi_j^0 S_k^- + \overline{\chi_i^0}(O_{L\,ij}^{ncs} P_L + O_{R\,ij}^{ncs} P_R)\chi_j^- S_k^+ \\
&+ \frac{1}{2}\overline{\chi_i^0}\gamma^\mu(O_{L\,ij}^{nnz} P_L + O_{R\,ij}^{nnz} P_R)\chi_j^0 Z_\mu^0 + \frac{1}{2}\overline{\chi_i^0}(O_{L\,ij}^{nnh} P_L + O_{R\,ij}^{nnh} P_R)\chi_j^0 H_k^0 \\
&+ \frac{i}{2}\overline{\chi_i^0}(O_{L\,ij}^{nna} P_L + O_{R\,ij}^{nna} P_R)\chi_j^0 A_k^0 \\
&+ \overline{\chi_i^-}\gamma^\mu(O_{L\,ij}^{cnw} P_L + O_{R\,ij}^{cnw} P_R)\chi_j^0 W_\mu^- + \overline{\chi_i^0}\gamma^\mu(O_{L\,ij}^{ncw} P_L + O_{R\,ij}^{ncw} P_R)\chi_j^- W_\mu^+ \\
&+ \overline{q_i}(O_{L\,ijk}^{qns} P_L + O_{R\,ijk}^{qns} P_R)\chi_j^0 \tilde{q}_k + \overline{\chi_i^0}(O_{L\,ijk}^{nqs} P_L + O_{R\,ijk}^{ncs} P_R) q_j \tilde{q}_k^*.
\end{aligned} \tag{49}$$

where the interesting couplings are given by:

$$O_{ij\,L}^{ncw} = -g(\mathcal{N}_{j2}U_{i1}^* + \frac{1}{\sqrt{2}}\mathcal{N}_{j3}\mathcal{U}_{i2}^* + \frac{1}{\sqrt{2}}\mathcal{N}_{j5}\mathcal{U}_{i3}^* + \frac{1}{\sqrt{2}}\mathcal{N}_{j6}\mathcal{U}_{i4}^* + \frac{1}{\sqrt{2}}\mathcal{N}_{j7}\mathcal{U}_{i5}^*) \tag{50}$$

$$O_{ij\,R}^{ncw} = -g(\mathcal{N}_{j2}^*\mathcal{V}_{i1} - \frac{1}{\sqrt{2}}\mathcal{N}_{j4}^*\mathcal{V}_{i2}), \tag{51}$$

with these couplings one can calculate the decay widths

$$\Gamma(\tilde{\chi}_1^0 \to \mu W) = \frac{1}{16\pi\ m_\chi^3}(|O_{41\,L}^{ncw}|^2 + |O_{41\,R}^{ncw}|^2)[(m_\chi^2 - (m_\mu + m_W)^2)(m_\chi^2 - (m_\mu - m_W)^2)]^{1/2}, \quad (52)$$

$$\Gamma(\tilde{\chi}_1^0 \to \tau W) = \frac{1}{16\pi\ m_\chi^3}(|O_{51\,L}^{ncw}|^2 + |O_{51\,R}^{ncw}|^2)[(m_\chi^2 - (m_\tau + m_W)^2)(m_\chi^2 - (m_\tau - m_W)^2)]^{1/2}, \quad (53)$$

the dependency on the alignment parameter Λ_2 in eq. 52 is hidden inside the matrices components $\mathcal{U}_{41}$, $\mathcal{U}_{42}$, $\mathcal{N}_{15}$, $\mathcal{N}_{16}$, $\mathcal{N}_{17}$, $\mathcal{N}_{14}$; with the matrix element $\mathcal{V}_{41}$ being zero. Similarly the dependecy on the alignment parameter Λ_3 in eq. 53 is hidden inside the matrices components $\mathcal{U}_{51}$, $\mathcal{U}_{52}$, $\mathcal{N}_{15}$, $\mathcal{N}_{16}$, $\mathcal{N}_{17}$, $\mathcal{N}_{14}$, with the matrix element $\mathcal{V}_{51}$ being zero too.

The connection between neutrino physics and collider physics given by BRPV susy is shown in the following equation

$$\boxed{\frac{\Lambda_2^2}{\Lambda_3^2} = \tan^2\theta_{\text{atm}} \approx \frac{\Gamma(\tilde{\chi}_1^0 \to \mu W)}{\Gamma(\tilde{\chi}_1^0 \to \tau W)}.} \quad (54)$$

The mSUGRA SU3 point

The channel chosen for this analysis is when a neutralino decays into a muon and a W boson, and after that, the W boson decays into two jets. This is the channel with the greatest branching ratio of all possible decays of this W boson.

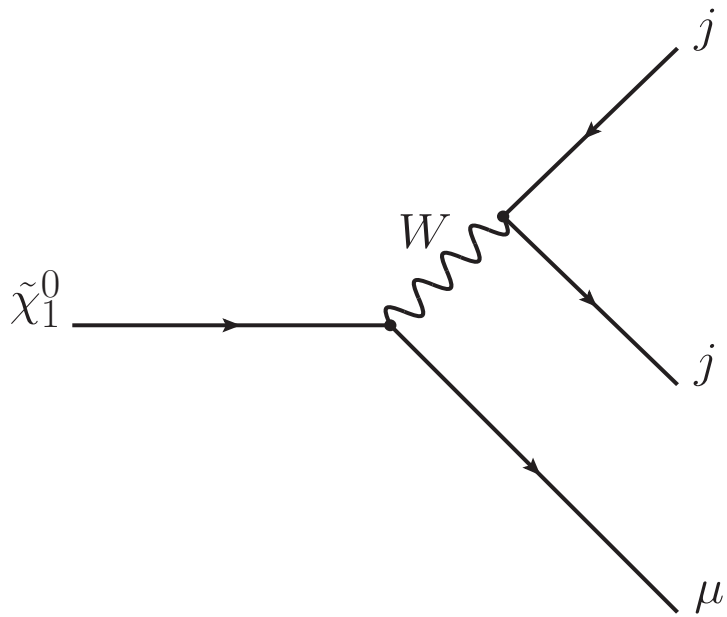

Figure: Decaying of a Neutralino into a W boson and a Muon. Then the W boson decays hadronically.

In this work an Atlasfast simulation of a BRPV susy point called SU3[1] was analyzed.

[1] No relation with group theory, it is just a name.

The mSUGRA SU3 point is defined by

$$\begin{array}{ll} m_0 = 100 \text{ GeV} & m_{1/2} = 300 \text{ GeV} \quad \tan\beta = 6 \\ A_0 = -300 \text{ GeV} & \text{sign}(\mu) = +1. \end{array} \tag{55}$$

The SPheno program was used for generate all the physical parameters of the model, then the event generation, and hadronization were done with Pythia, then simulation, digitation and reconstruction were done with the Atlfast software.
The most relevant parameters are the neutrino mass differences and mixing angles, this comes from theoretical predictions on neutrino physics:

$$\begin{array}{ll} \Delta m^2_{\text{atm}} = 2.2 \times 10^{-3} \text{ eV}^2 & \Delta m^2_{\text{sol}} = 2.8 \times 10^{-5} \text{ eV}^2 \\ \tan^2\theta_{\text{atm}} = 0.96 & \tan^2\theta_{\text{sol}} = 0.64, \end{array} \tag{56}$$

and the free parameters, that are input parameters for SPheno:

$$\begin{array}{ll} \epsilon_1 = -\epsilon_2 = \epsilon_3 = 102 \text{ MeV} & v_1 = -8.8 \text{ MeV} \\ v_2 = 9.0 \text{ MeV} & v_3 = -8.6 \text{ MeV}. \end{array} \tag{57}$$

In this BRPV susy point the Lightest Supersymmetric Particle LSP is the lightest neutralino, with a mass of $m_{\chi_1^0} = 118$ GeV and a lifetime of $c\tau = 290\,\mu$m. The cross section was of 1.4 pb^{-1} and 9969 events were generated. The branching ratios for the neutralino decay modes in the BRPV SU3 point are

$$\begin{array}{ll} BR(\tilde{\chi}_1^0 \rightarrow \mu W) = 10.3\% & BR(\tilde{\chi}_1^0 \rightarrow \nu\tau\tau) = 29.8\% \\ BR(\tilde{\chi}_1^0 \rightarrow \tau W) = 11.0\% & BR(\tilde{\chi}_1^0 \rightarrow \nu\tau\mu) = 14.8\% \\ BR(\tilde{\chi}_1^0 \rightarrow \nu Z) = 8.3\% & BR(\tilde{\chi}_1^0 \rightarrow \nu\tau e) = 14.8\%. \end{array} \quad (58)$$

The channel $\tilde{\chi}_1^0 \rightarrow \tau W$ was not explored in this work since the 2010 data with integrated luminosity of 35 pb^{-1} did not produce sufficent taus in order to do a physics analysis; so have sought in the channel $\tilde{\chi}_1^0 \rightarrow \mu W$ was really an early and fascinating BRPV susy search!

ATLAS

In general the ATLAS detector has axial symmetry, around the beam axis,

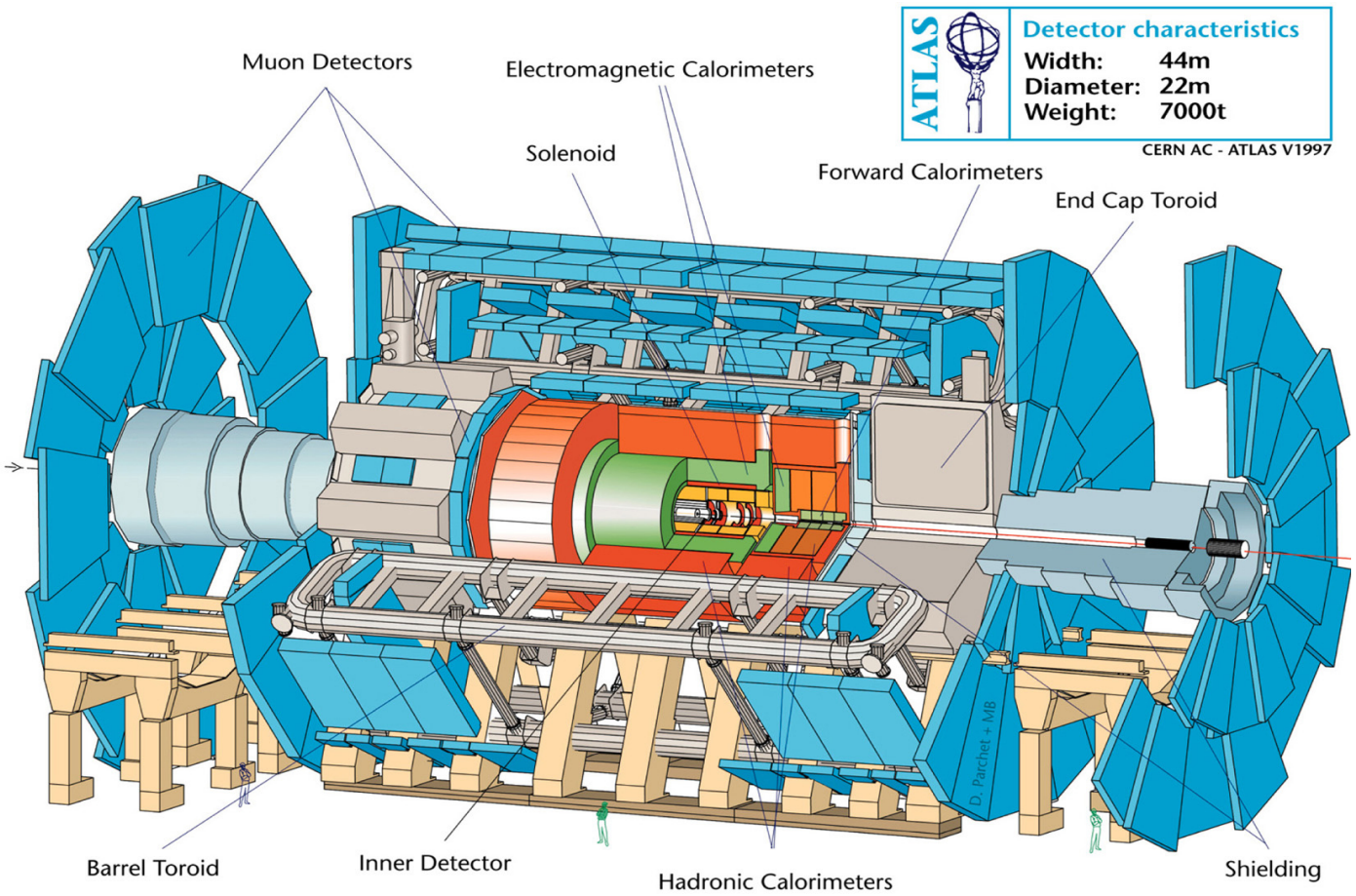

Figure: A Toroidal LHC Aparatus.

so that cyllindrical coordinates (ct, ρ, ϕ, z) are widely used to describe the kinematic variables e.g. the momentum of a particle is expressed as: $(\frac{E}{c}, p_\rho, p_\phi, p_z)$. Is worth to say that the azimutal angle ϕ varies between $(-\pi, \pi]$. At different subdetectors levels other coordinate systems are used, among these, the cartesian, the spherical, and not properly a coordinate system, the detector system coordinates[2]. The cartesian coordinate system is mobile around the Large Hadron Collider LHC, and in particular at the center of the ATLAS detector has its x axis aiming to the center of the LHC ring, the z axis along the beam direction, and the y axis aiming to the sky. Spherical coordinates stays as usual. The detector variables serves to define the 4-momentum of a particle. These are: the transverse momentum magnitude, pseudorapidity, azimutal angle, and energy.

[2] Also called the detector variables

Transverse Momentum Magnitude p_T: The transverse momentum is the component of the three-vector momentum perpendicular to the beam axis, and is used in the tracking detectors of ATLAS (Inner Detector, and Muon Spectrometer). In the ATLAS detectors that use calorimetry the transverse energy $E_T = cp_T$ is used instead of p_T. The three-vector momentum is $\vec{p} = \vec{p}_T + \vec{p}_z$, and the transverse momentum is

$$\vec{p}_T = p_x\vec{e}_x + p_y\vec{e}_y = p_\rho\vec{e}_\rho + p_\phi\vec{e}_\phi. \tag{59}$$

The magnitude of this two-component vector $|p_T|$ is equals to p_ρ.

Pseudorapidity η: The pseudorapidity is an angular variable defined by

$$\eta = -\ln\left(\tan\left(\frac{\theta}{2}\right)\right), \tag{60}$$

with θ, the polar spherical angle. The pseudorapidity is ∞ at $\theta = \pi$ and $-\infty$ at $\theta = -\pi$.
Azimutal angle ϕ: This is the ϕ of cyllindrical coordinates. It varies between $(-\pi, \pi]$.
Energy E: This is the particle's energy.

With these four detector variables, one can form the four-vector momentum of any particle by:

$$\begin{aligned} p_x &= p_T \cos\phi \\ p_y &= p_T \sin\phi \\ p_z &= p_T \sinh\eta \\ E &= E \end{aligned} \tag{61}$$

Definitions

Event: In this work an event is an ATLAS event, and is the result of the collision of two bunches of protons.
Global Variable: A global variable is one that has a one-to-one correspondence with the number of events, i.e. a global variable has one and only one value per event.
Leading Particle: A leading particle is a particle that has the highest transverse momentum in a event. In the same way a particle that has the second highest transverse momentum is said to be a subleading particle, e.g. the statement "the three leading jets" means the three jets in the event with the highest p_T.
Angular Distance ΔR: The angular distance between two particles 1 and 2 is

$$\Delta R(1,2) = \sqrt{(\eta_1 - \eta_2)^2 + (\phi_1 - \phi_2)^2}. \tag{62}$$

The difference in ϕ is calculated modulo π.

Missing Transverse Energy $\not{E}_T$: In collider physics, when the protons are travelling, the initial momentum along the transverse plane is zero, so the presence of momentum in the transverse plane guarantees the existence of missing energy transverse ($|\vec{p}| = E/c$), that is the vector sum of the tranverse energy of all fermions; and is thought to belong to undetectable particles e.g. neutrinos. Experimentally one has to sum over the energy's deposits in the calorimeter towers:

$$\vec{\not{E}}_T = \sum_i^N E_T^i \hat{n}_i, \tag{63}$$

with $\hat{n}_i$ an unitary perpendicular vector to the beam axis, and N the number of calorimeter towers. Obviously $\not{E}_T$ is the norm of $\vec{\not{E}}_T$.

Transverse Sphericity S_T: Let $\vec{Q}_x$ be an array whose components are the x momentum component of all fermions, similarly let $\vec{Q}_y$ be an array whose components are the y momentum component of all fermions; then the sphericity matrix is defined as:

$$S = \begin{pmatrix} \vec{Q}_x \cdot \vec{Q}_x & \vec{Q}_x \cdot \vec{Q}_y \\ \vec{Q}_y \cdot \vec{Q}_x & \vec{Q}_y \cdot \vec{Q}_y \end{pmatrix}, \tag{64}$$

with eigenvalues λ_- and λ_+. The transverse sphericity is a global variable, it was introduced by Bjorken and is defined as:

$$S_T = \frac{2\lambda_-}{\mathrm{Tr}(S)}. \tag{65}$$

S_T is nearly to 0 for QCD events (diffractive scattering), and is close to 1 for spherical events. Supersymmetric events are guessed to be spherical, due that these events need to be produced at high energies, therefore the most of the particles will yield in the transverse plane.

Transverse Scalar Mass H_T: This global variable could be defined in different ways, i.e. it is analysis dependent. In this work it is defined as the sum of the transverse momentum magnitude of all muons plus the transverse momentum magnitude of the three leading jets in the event. If the number of jets is less than three, then the p_T of all jets are added. Since that the channel in this work involves at least two jets, a choice for a transverse scalar mass involving two jets or more, instead of three jets or more, could be done, but with the choice made here, the additional jet requiered help us to remove the abundant QCD dijet background. The transverse scalar mass is:

$$H_T = \begin{cases} \sum_{\mu_i=0}^{n_\mu-1} p_T^{\mu_i} + \sum_{i=0}^{n_j-1} p_T^{j_i} & \text{if } n_j < 3 \\ \sum_{\mu_i=0}^{n_\mu-1} p_T^{\mu_i} + \sum_{i=0}^{3-1} p_T^{j_i} & \text{if } n_j \geq 3 \end{cases}, \tag{66}$$

with n_j the number of jets in the event, n_μ the number of muons in the event; and the particle's labels are taken *a la* C++[3].

[3] In C++ the arrays are labeled starting at 0 and ending at its size minus one.

Effective Mass M_{eff}: The effective mass is defined as the sum between the scalar transverse mass and the missing energy transverse mass.

$$M_{\text{eff}} = H_T + \not{E}_T, \tag{67}$$

and of course it is a global variable.
Transverse Mass M_T: The transverse mass is defined as:

$$M_T^{\mu_i} = \sqrt{2 \cdot p_T^{\mu_i} \cdot \not{E}_T \cdot (1 - \cos(\phi^{\mu_i} - \phi^{\not{E}_T}))}, \tag{68}$$

in this analysis it is not a global variable because in this analysis events with more than one muon were taken. When one parent particle decays to one visible and one invisible daughter particle, this variable is useful to deal with the $W \to l\nu + jets$ background, and also serves as a discriminant variable for R parity conserving searches. The $M_T^{\mu_i}$ drops its upper index by commodity and become M_T.

Inner Detector

The ID is immersed in a 2 T magnetic field generated by the central solenoid, which extends over a length of 5.3 m with a diameter of 2.5 m.

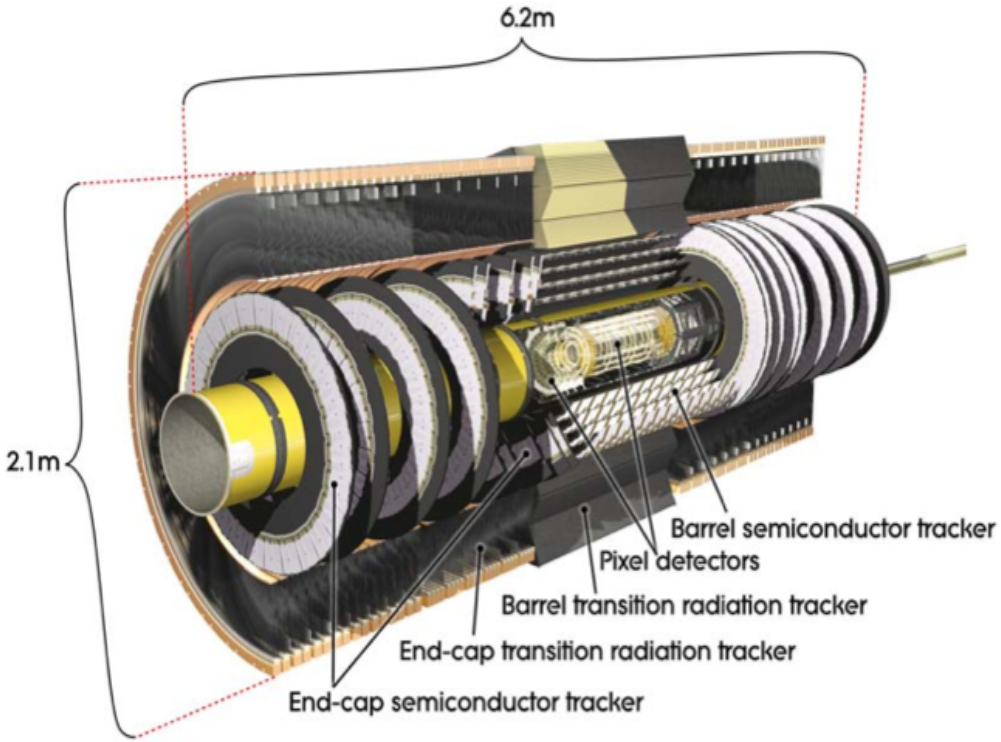

Figure: Split overview of the Inner Detector.

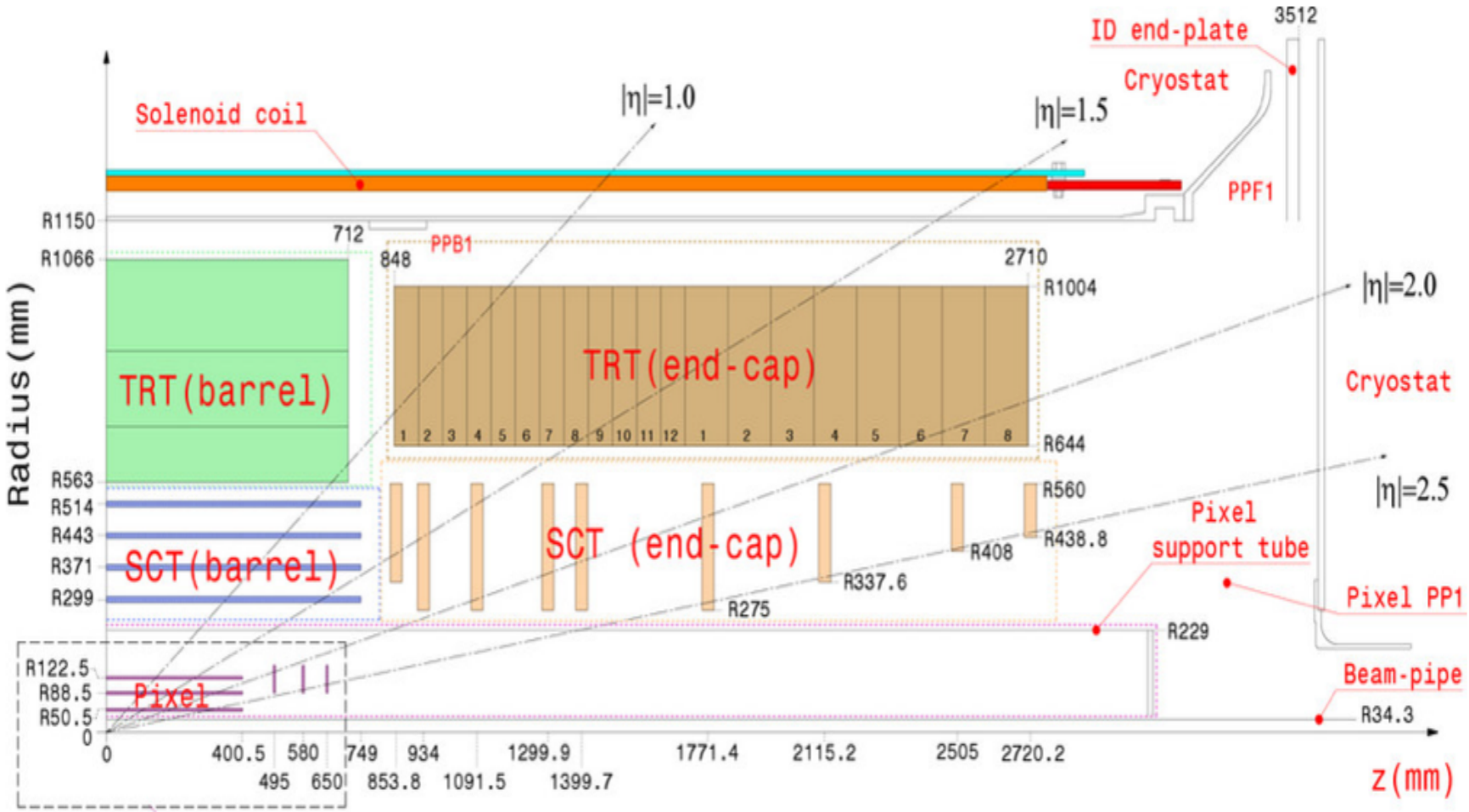

Figure: ρ vs z view of the ID with its subparts and dimensions.

Item		Radial extension (mm)	Length
Pixel	Overall envelope	$45.5 < R < 242$	$0 < \|z\| < 3092$
3 cylindrical layers	Sensitive barrel	$50.5 < R < 122.5$	$0 < \|z\| < 400.5$
2×3 disks	Sensitive end-cap	$88.8 < R < 149.6$	$495 < \|z\| < 650$
SCT	Overlap envelope	$255 < R < 549$ (barrel)	$0 < \|z\| < 805$
		$251 < R < 610$ (end-cap)	$810 < \|z\| < 2797$
4 cyllindrical layers	Sensitive barrel	$299 < R < 514$	$0 < \|z\| < 749$
2×9 disks	Sensitive end-cap	$275 < R < 560$	$839 < \|z\| < 2735$
TRT	Overall envelope	$574 < R < 1082$ (barrel)	$0 < \|z\| < 780$
		$617 < R < 1106$ (end-cap)	$827 < \|z\| < 2744$
73 straw planes	Sensitive barrel	$563 < R < 1066$	$0 < \|z\| < 712$
160 straw planes	Sensitive end-cap	$644 < R < 1004$	$848 < \|z\| < 2710$

Table: Inner detector parameters.

Calorimetry

$$\text{Calorimetry} = \begin{cases} \text{EM Calorimeter EMC} \begin{cases} \text{Presampler} \\ \text{Sampling 1} \\ \text{Sampling 2} \\ \text{Sampling 3} \end{cases} \\ \text{Hadronic Calorimeter HC} \begin{cases} \text{Tile Calorimeter ITC} \\ \text{LAr Hadronic Cal.} \begin{cases} \text{End-Cap HEC} \\ \text{Barrel} \\ \text{Forward FCAL} \end{cases} \end{cases} \end{cases}$$

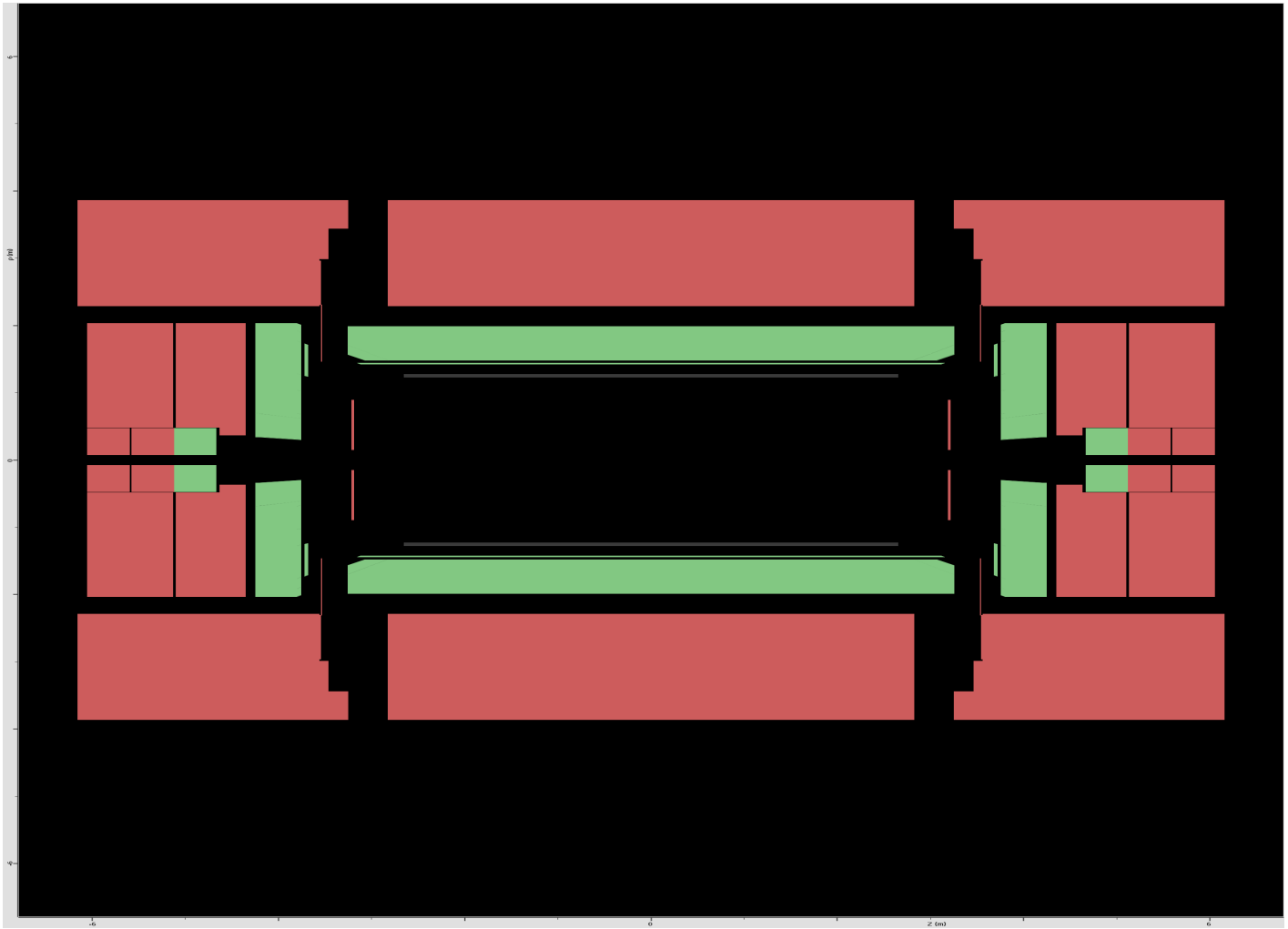

Figure: Calorimetry ρz plane. Green: LAr Detectors. Red: Tile Detectors.

Muon Spectrometer

Cathode Strip Chamber CSC: non-flamable gas 30% Ar, 50% CO_2, 20% CF_4
Resistive Plate Chamber RPC: non-flamable and enviromental gas $C_2H_2F_4$ (tretrafluoeratano) and a little of SF_6. Plates of bakelite. Every chamber contains two layer detectors and four readout systems.
Thin Gap Chamber TGC: highly flammable gas 55% CO_2 and 45% $n - C_5H_{12}$ (n-Pentane). Small sensitivity to mechanical deformations.
Monitored Drift Tubes Aluminium tubes (3 cm diameter and 400μm wall thickness) with a center of thungsten-rhenium (50μm diameter). In the middle of the aluminium and the thungsten-rhenium there is a gas mixture of 93% Ar and 7% CO_2. The lentghs of the tubes varies between 70 cm to 630 cm.

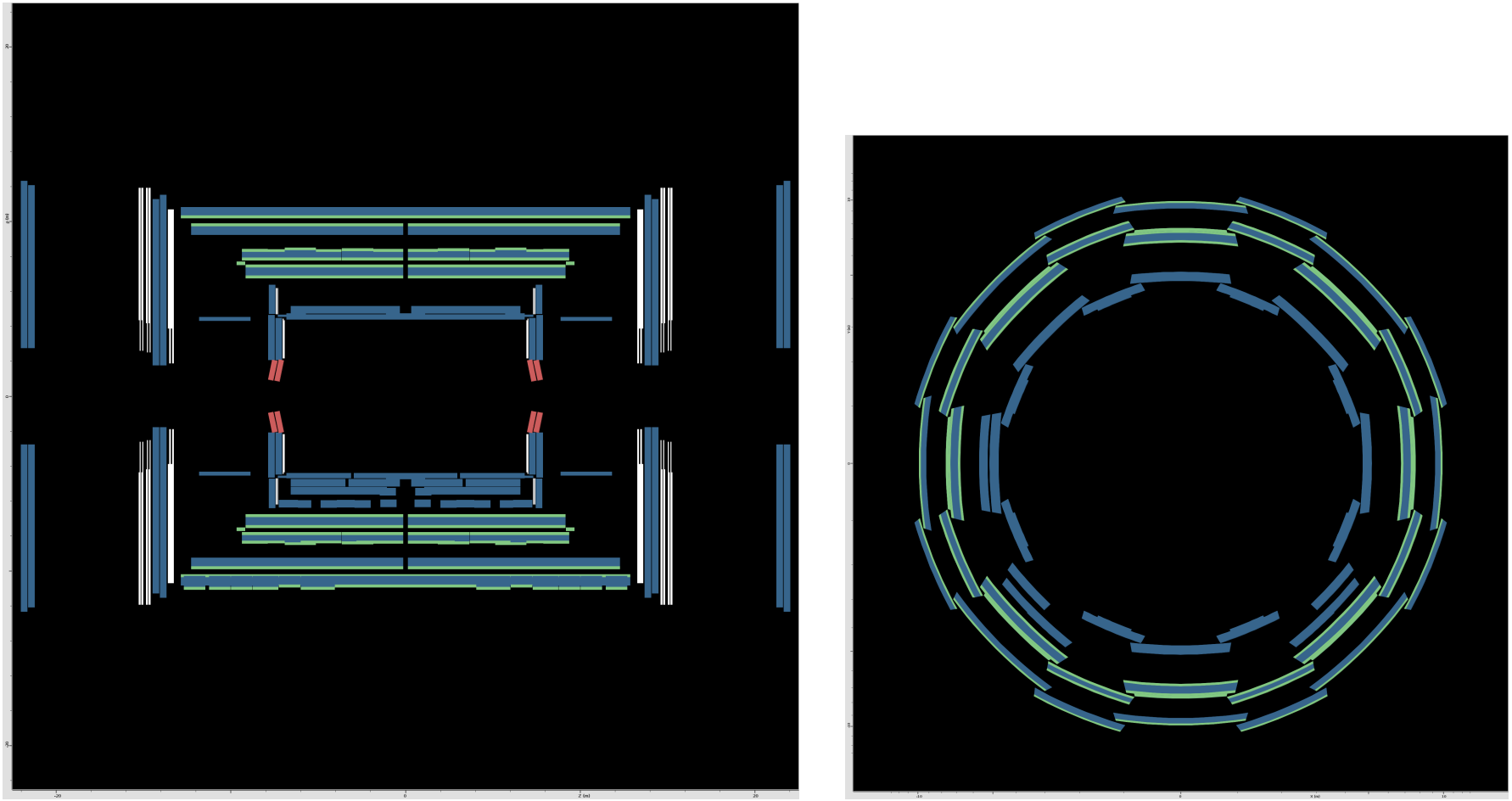

Figure: Muon spectrometer subsystems. Green: RPC, Blue: MDT, White: TGC, Red: CSC.

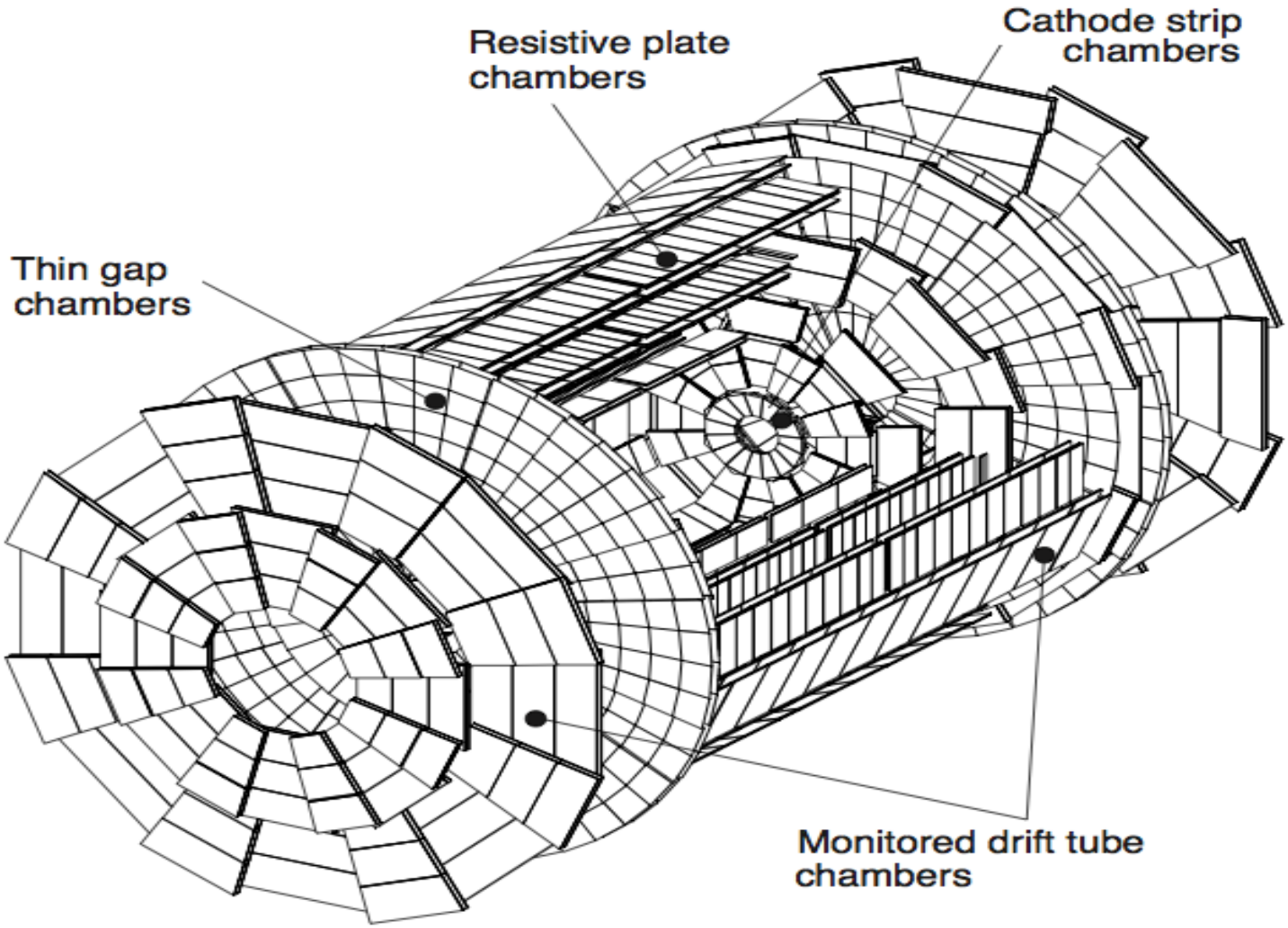

Figure: Muon spectrometer subsystems.

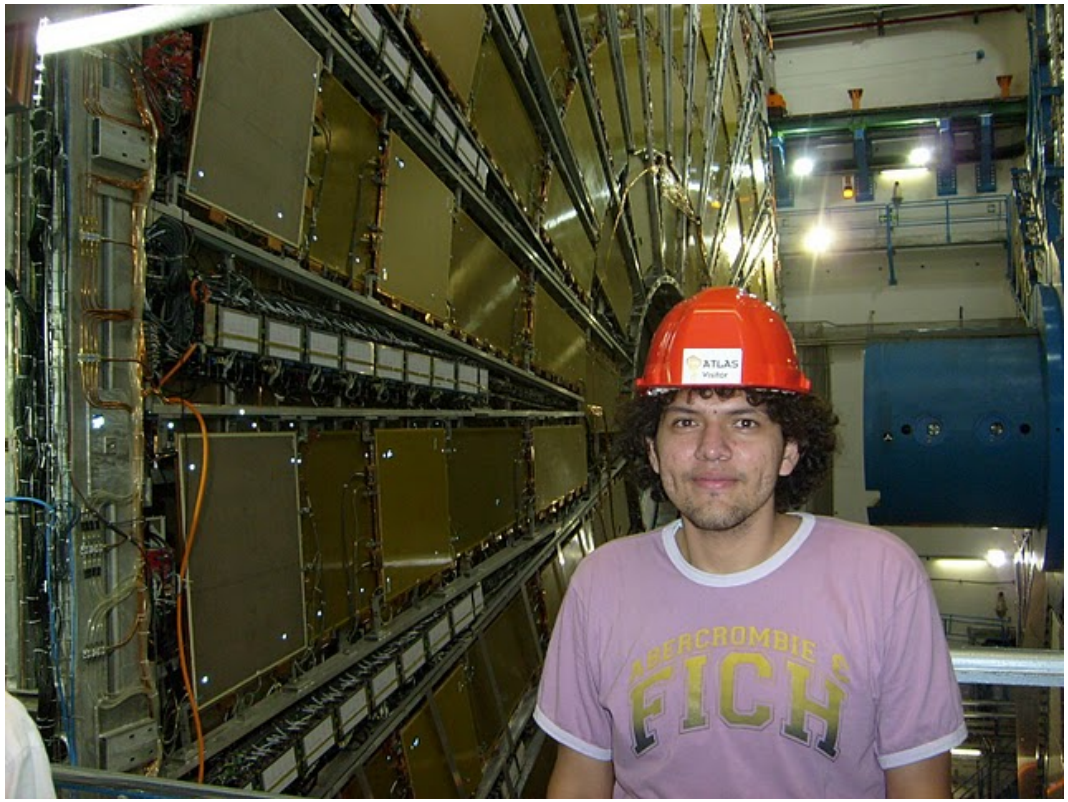

Figure: Real photograph of the MDT End-Cap.

Trigger

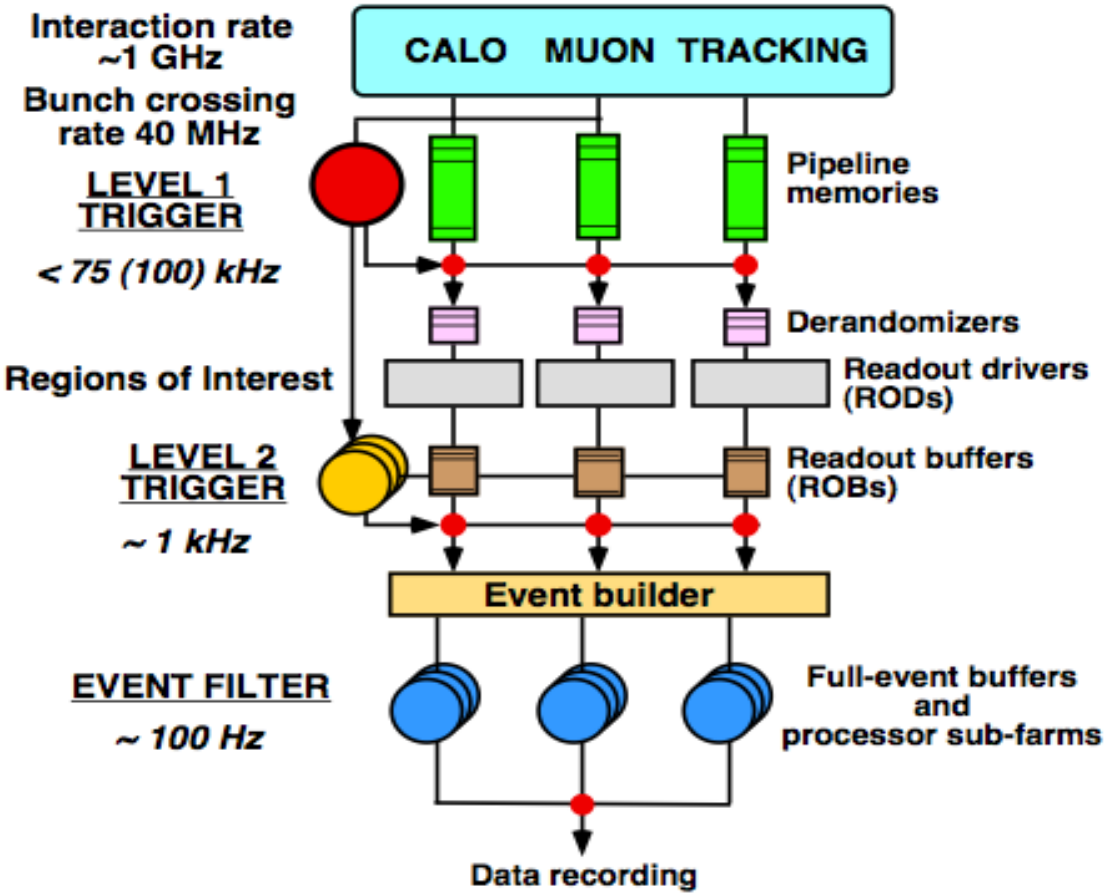

Figure: Trigger scheme.

Working Service

Before to start to take advantage of the CERN facilities, the student have to do a *working service*. This working service is a work that the student does to maintain the machine in a good state. There are a lot of modalities to provide a working service. The most common are: the validation of algorithms, and the shifts to guard either the ATLAS subsystems, or the GRID. During this thesis the validation group (including myself) realized a validation of the algorithms that run every night in ATLAS for the ATLAS high-level trigger. I was included in this project in the period between May of 2008, and October of 2008 (the time of my internship at CERN). This work ends with a publication: *Software validation infrastructure for the ATLAS high-level trigger, PoS ACAT08 084.*

The LHC experiment produce between 10 to 15 petabytes per year, so data must be stored on a common site and no replication of data is strictly necessary. For that purpose the GRID was created. The GRID are clouds of supercomputers connected among them with the idea that user software is sending to the petabytes and not backwards. The GRID have three principal levels of mirroring (replicating) data called Tiers. The principal the Tier zero (T0) is located at CERN (Switzerland and France) and stored all the real data and montecarlos, then the data is sent to ten computer clouds around the world called Tiers one (T1). These T1 are: CA (Canada), DE (Deutchsland), ES (España), FR (France, Japan, and Beijing), IT (Italy), ND (Norway, Sweden, and Switzerland), NL (Netherlands and Rusia), TW (Taiwan), UK (United Kingdom), and US (United States of America). The Tiers two (T2) are located around the world, and in general have not all the data, but a big portion of them. These T2 in general are inside countries with T1, and emerging countries as Brasil. Finally there is a new kind of Tier, the Tier 3, these T3 are located in either countries with less money or with less interest in High Energy Physics research.

Examples of T3 in our region are: UNIANDES (Colombia), UAN (Colombia), UTFSM (Chile). Today the Pontificia Universidad Católica de Chile (PUC) is trying to start up a T3. Without the GRID I had not been able to process the data used in this thesis. Also without the server called "nyx" at PUC, I had not been able to analyze the processed data comming from the GRID.
ATLAs Distributed Computing operational Shifts (ADCoS),
https://twiki.cern.ch/twiki/bin/viewauth/Atlas/ADCoS
is a work consisting in monitoring the GRID by shifts of eight hours. During a day there are three shifts covering the 24 hours of activity of the GRID. By commodity the shifts are reparted in three continents: Americas, Europe, and Asia. It is also worth to say that during a shift, there are three shifters, the expert, the senior, and the trainee. During these shifts the shifter must to watch/guard the grid (mostly T0, T1, and T2) and try to catch errors due to transference, storage, invalid credentials, memory segmentation, and performance of the CERN databases. When an error is catched, the shifter must report the error, and fix the problem by (him/her)self or by calling to the expert on call. In my doctorate I took 56 shifts in the period between 2008 and 2010.

MC samples

We want to do histograms of kinematic variables comparing real data, the MCB, and the signal region. Since that the real data is at 35 pb^{-1}, we have to scale the montecarlo samples luminosity by

$$\alpha_i \times L_i = 35 pb^{-1}, \tag{69}$$

with α_i the scale factor for montecarlo sample i, and L_i their integrated luminosity. Given that the number of events for a montecarlo sample is

$$N_i = \sigma_{\text{eff},i} \times L_i, \tag{70}$$

with $\sigma_{\text{eff},i}$ the effective cross section, the luminosity scale factor to every montecarlo background is:

$$\alpha_i = \frac{35 pb^{-1} \sigma_{\text{eff},i}}{N_i}. \tag{71}$$

The luminosity scale factor α_i enters as a weight when the histograms are filled. Note that the luminosity scale factors for the backgrounds that form the QCD MCB, are greater than one, while the luminosity scale factors for the rest of the backgrounds, are less than one. When we look for a kinematic selection such that the sum of all the MCB coincide with the real data, the luminosity scale factors will be rescaled in order to fulfill this requeriment.

MC Code	Physics	Pile-up	Events	σ_{eff} [pb]
105009	J0_pythia_jetjet		1379184	975297e4
105010	J1_pythia_jetjet		1395383	67302e4
105011	J2_pythia_jetjet		1398078	41194700
105012	J3_pythia_jetjet		1397430	2193250
105013	J4_pythia_jetjet		1397401	87848.7
105014	J5_pythia_jetjet		1391612	2328.56
105015	J6_pythia_jetjet		1347654	33.8461
105016	J7_pythia_jetjet		1125428	0.13741

Table: QCD MCB used in this work.

MC Code	Physics	Pile-up	Events	σ_{eff} [pb]
105985	WW_Herwig		249837	44.9*0.3884
105986	ZZ_Herwig		249725	5.96*0.2123
105987	WZ_Herwig		249830	18.0*0.3085

Table: dibosons MCB used in this work.

MC Code	Physics	Pile-up	Events	σ_{eff} [pb]
105200	T1_McAtNlo_Jimmy		999387	160.79*0.556

Table: ttbar MCB used in this work.

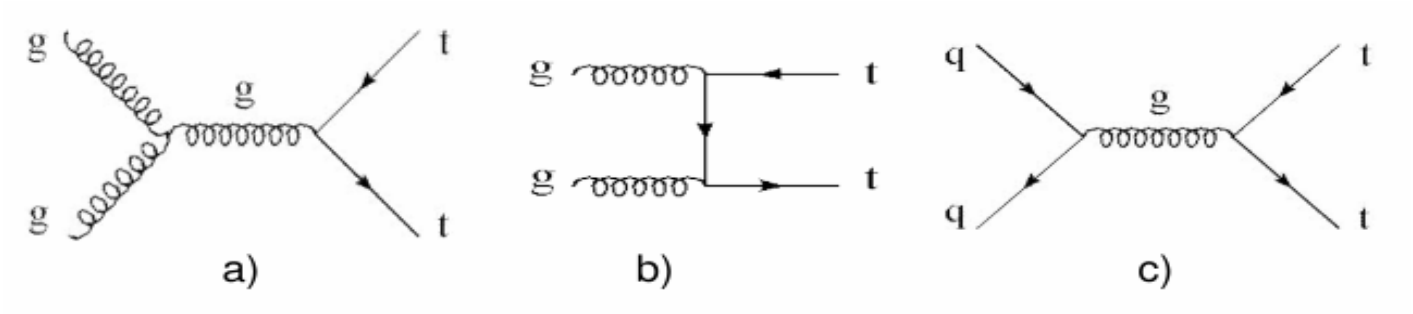

Figure: Top production processes at lowest order: gluon-gluon scattering diagrams (a) and (b) and quark-quark scattering diagram (c).

MC Code	Physics	Pile-up	Events	σ_{eff} [pb]
108340	st_tchan_enu_McAtNlo_Jimmy		9993	7.00
108341	st_tchan_munu_McAtNlo_Jimmy		9997	7.00
108342	st_tchan_taunu_McAtNlo_Jimmy		10000	7.00
108343	st_schan_enu_McAtNlo_Jimmy		9950	0.468
108344	st_schan_munu_McAtNlo_Jimmy		9996	0.468
108345	st_schan_taunu_McAtNlo_Jimmy		9996	0.468
108346	st_Wt_McAtNlo_Jimmy		14995	13.00

Table: single top MCB used in this work.

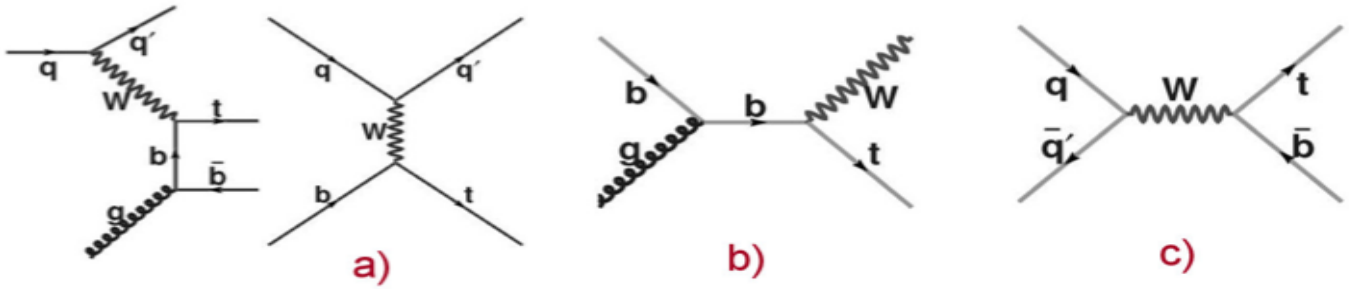

Figure: Main graphs corresponding to the three production mechanisms of single-top quark events: (a) t-channel (b) Wt associated production (c) s-channel.

MC Code	Physics	Pile-up	Events	σ_{eff} [pb]
106280	AlpgenJimmyWbbNp0_pt20		6499	3.2*1.22
106281	AlpgenJimmyWbbNp1_pt20		5500	2.6*1.22
106282	AlpgenJimmyWbbNp2_pt20		2997	1.4*1.22
106283	AlpgenJimmyWbbNp3_pt20		1500	0.6*1.22
107680	AlpgenJimmyWenuNp0_pt20		1381531	6913.3*1.19887
107681	AlpgenJimmyWenuNp1_pt20		257958	1293.0*1.19887
107682	AlpgenJimmyWenuNp2_pt20		188896	377.1*1.19887
107683	AlpgenJimmyWenuNp3_pt20		49978	100.9*1.19887
107684	AlpgenJimmyWenuNp4_pt20		12991	25.3*1.19887
107685	AlpgenJimmyWenuNp5_pt20		3449	6.9*1.19887
107690	AlpgenJimmyWmunuNp0_pt20		1386038	6913.3*1.19887
107691	AlpgenJimmyWmunuNp1_pt20		254959	1293.0*1.19887
107692	AlpgenJimmyWmunuNp2_pt20		187860	377.1*1.19887
107693	AlpgenJimmyWmunuNp3_pt20		49887	100.9*1.19887
107694	AlpgenJimmyWmunuNp4_pt20		12991	25.3*1.19887
107695	AlpgenJimmyWmunuNp5_pt20		3498	6.9*1.19887
107700	AlpgenJimmyWtaunuNp0_pt20		1364841	6913.3*1.19887
107701	AlpgenJimmyWtaunuNp1_pt20		254753	1293.0*1.19887
107702	AlpgenJimmyWtaunuNp2_pt20		187946	377.1*1.19887
107703	AlpgenJimmyWtaunuNp3_pt20		49972	100.9*1.19887
107704	AlpgenJimmyWtaunuNp4_pt20		12996	25.3*1.19887
107705	AlpgenJimmyWtaunuNp5_pt20		3498	6.9*1.19887

Table: W Boson samples used in this work.

MC Code	Physics	Pile-up	Events	σ_{eff} [pb]
107650	AlpgenJimmyZeeNp0_pt20		303966	830.125
107651	AlpgenJimmyZeeNp1_pt20		63440	166.2375
107652	AlpgenJimmyZeeNp2_pt20		18997	50.2825
107653	AlpgenJimmyZeeNp3_pt20		5499	13.9225
107654	AlpgenJimmyZeeNp4_pt20		1499	3.615625
107655	AlpgenJimmyZeeNp5_pt20		500	0.9417875
107660	AlpgenJimmyZmumuNp0_pt20		303947	830.125
107661	AlpgenJimmyZmumuNp1_pt20		62996	166.2375
107662	AlpgenJimmyZmumuNp2_pt20		18993	50.2825
107663	AlpgenJimmyZmumuNp3_pt20		5497	13.9225
107664	AlpgenJimmyZmumuNp4_pt20		1499	3.615625
107665	AlpgenJimmyZmumuNp5_pt20		499	0.9417875
107770	AlpgenJimmyZtautauNp0_pt20		302959	830.125
107771	AlpgenJimmyZtautauNp1_pt20		62981	166.2375
107772	AlpgenJimmyZtautauNp2_pt20		18993	50.2825
107773	AlpgenJimmyZtautauNp3_pt20		5497	13.9225
107774	AlpgenJimmyZtautauNp4_pt20		1499	3.615625
107775	AlpgenJimmyZtautauNp5_pt20		499	0.9417875
108319	PythiaDrellYan_mumu		999503	1252.9
108320	PythiaDrellYan_ee		999969	1253.0
108321	PythiaDrellYanLowM_mu3		499925	4407.0*0.51
108322	PythiaDrellYanLowM_ee3		499925	4406.1*0.50

Table: Z Boson samples used in this work. A k factor of 1.25 was already included in the cross section for consistency with the NNLO value.

MC Code	Physics	Pile-up	Events	σ_{eff} [pb]
114010	Pythia_bRPV_SU3		9969	1.4086

Table: BRPV SU3 signal sample properties.

Object Defs.

Missing Transverse Energy: The missing transverse energy used in this analysis (algorithm SimplifiedRefFinal) is the magnitude of the vectorial sum of reconstructed objects in the event, namely

1. the jets calibrated at electromagnetic jet energy scale EMJES with at least $p_T > 20$ GeV,
2. the muons of the signal,
3. the additional potential nonisolated muons (muons with transverse momentum less than 1.8 GeV inside a cone of $\Delta R \leq 0.2$),
4. the topological calorimeter clusters not belonging to pre-cited objects (CellOut term) calibrated as the EM scale.

Muon			
Cut	Value	MC	Data
Smearing	smearing from performance group		
Algorithm	STACO, combined and low p_T reconstructed no combined or χ^2(match)<150 no combined or $p_T^{MS} \geq 50$ GeV or $p^{MS} > 0.6 p^{ID}$		
Acceptance	$p_T > 20$ GeV or $\lvert\eta\rvert < 2.4$		
Inner Detector Track Quality	$n_{PIXEL}^{hits} \geq 1$ or $n_{SCT}^{hits} \geq 6$ $\lvert\eta\rvert < 1.9$ or $n_{TRT}^{hits+outliers} \geq 6$ $n_{TRT}^{hits+outliers} \leq 6$ or $n_{TRT}^{outliers} < 0.9\, n_{TRT}^{hits+outliers}$		
Track Isolation	$\sum p_T < 1.8$ GeV (in a $\Delta R \leq 0.2$)		
Overlap Removal	if $\Delta R(\mu, jet) < 0.4$, reject muon and kept jet		
Cosmics	no event veto if $\lvert z_\mu - z_{PV}\rvert < 10$mm		

Table: Muon object definition.

If a jet and a muon are close $\Delta R(\mu, j) < 0.4$, then the muon is rejected and the jet is kept in order to avoid to take fake muons, e.g. kaons and B mesons.

A bad loose jet is defined by:

1. Electromagnetic coherent noise: em fraction (electric charge fraction) > 0.95 and $|Q| > 0.8$ where Q is the jet quality based on liquid argon cell pulse shapes [$Q = 0(1)$ means high (very low) quality]. Jet quality is the fraction of LAr cells with a Q-factor greater than 4000. The cell Q-factor measures the difference between the measured pluse shape (a_i^{measured}) and the predicted pulse shape ($a_i^{\text{predicted}}$) that is used to reconstruct the cell energy. It is computed as $\sum_{\text{samples}}(a_i^{\text{measured}} - a_i^{\text{predicted}})^2$ and is stored as 16-bit integer.
2. HEC spike: hec fraction (jet energy fraction in the HEC) > 0.8, and $n_{90} \leq 5$ or hec fraction > 0.5 and $|Q| > 0.5$. The variable n_{90} is the minimum number of cells containing at least 90% of the jet energy;
3. Cosmic beam background: the timing must satisfy $|t| > 25$ ns, or em fraction < 0.05 or Fmax > 0.99. Fmax is the maximum energy fraction in one calorimeter layer and $|\eta| < 2$. The timing is calculated using cells, and is energy squared weighted $t = \sum_i E_i^2 t_i / \sum_i E_i^2$.

Given the very low frequency of this bad jet appearance, the event containing at least one of this jet with $p_T > 20$ GeV is removed for the analysis. This corresponds to less than one per mill in a typical SUSY signal as well as in data. Note that the p_T requirement for the three jets to enter the analysis is tightened to 30 GeV, while the transverse momentum of the leading jet must exceed 60 GeV. To finalize a jet that pass the b-tagging is a good jet that has a weight flavor greater than 5.72. The jet energy resolution have been measured with di-jet balance and bisector techniques. To match the data, an additional jet energy smearing is required. It consists of a Gaussian distribution with a p_T-dependent resolution function

$$0.55\sqrt{\frac{(4.6\ \text{GeV})^2}{p_T^2} + \frac{0.846^2\ \text{GeV}}{p_T} + 0.064^2} \tag{72}$$

and gives an additional 12 % (8 %) for a p_T of 30 GeV (60 GeV).

Jet			
Cut	Value	MC	Data
Algorithm	AntiKt4H1Topo		
Acceptance	$p_T > 20$ GeV or $\lvert\eta\rvert < 2.5$		
Veto	reject events with bad loose jets		
Smearing	smearing of jet uncertainties		
Overlap Removal	if $\Delta R(\mu, jet) < 0.4$, reject muon and kept jet if $0.2 < \Delta R < 0.4$, reject electron and kept jet if $\Delta R < 0.2$, reject jet and kept electron		
b-jet	if jet weight flavor is > 5.72, the jet is a b-jet		

Table: Jet object definition.

Electron			
Cut	Value	MC	Data
Algorithm	AuthorElectron		
Acceptance	$p_T > 20$ GeV or $\lvert\eta^{cluster}\rvert < 2.47$		
Quality	Robust Medium and no touching a dead OTX		
Overlap Removal	if $0.2 < \Delta R < 0.4$, reject electron and kept jet if $\Delta R < 0.2$, reject jet and kept electron		

Table: Electron object definition.

BRPV KS

The events selected for this analysis were primarily used to calibrate the standard model background with the real data. A scale factor of 0.55 on the QCD (dijet) samples was found to calibrate the missing energy transverse $\not\!\!E_T$. The set of cuts or requeriments on some variables to this purpouse were:

1. the request that all the primary vertices of the events had at least five tracks,
2. the request that there was not bad loose jets,
3. the presence of one or more muons per event,
4. the rejection of events with cosmic muons,
5. the presence of three or more jets per event,
6. the presence of a leading jet with transverse momentum $p_T > 60$ GeV, a subleading jet with a $p_T > 30$ GeV, and a subsubleading jet had a $p_T > 30$ GeV,
7. and the requeriment that the azimutal angle of the three leading jets were apart from the $\phi_{\not\!\!E}$ by 0.2 rad.

Henceforth the above selection will be called the BRPV Kinematic Selection (BRPV KS).

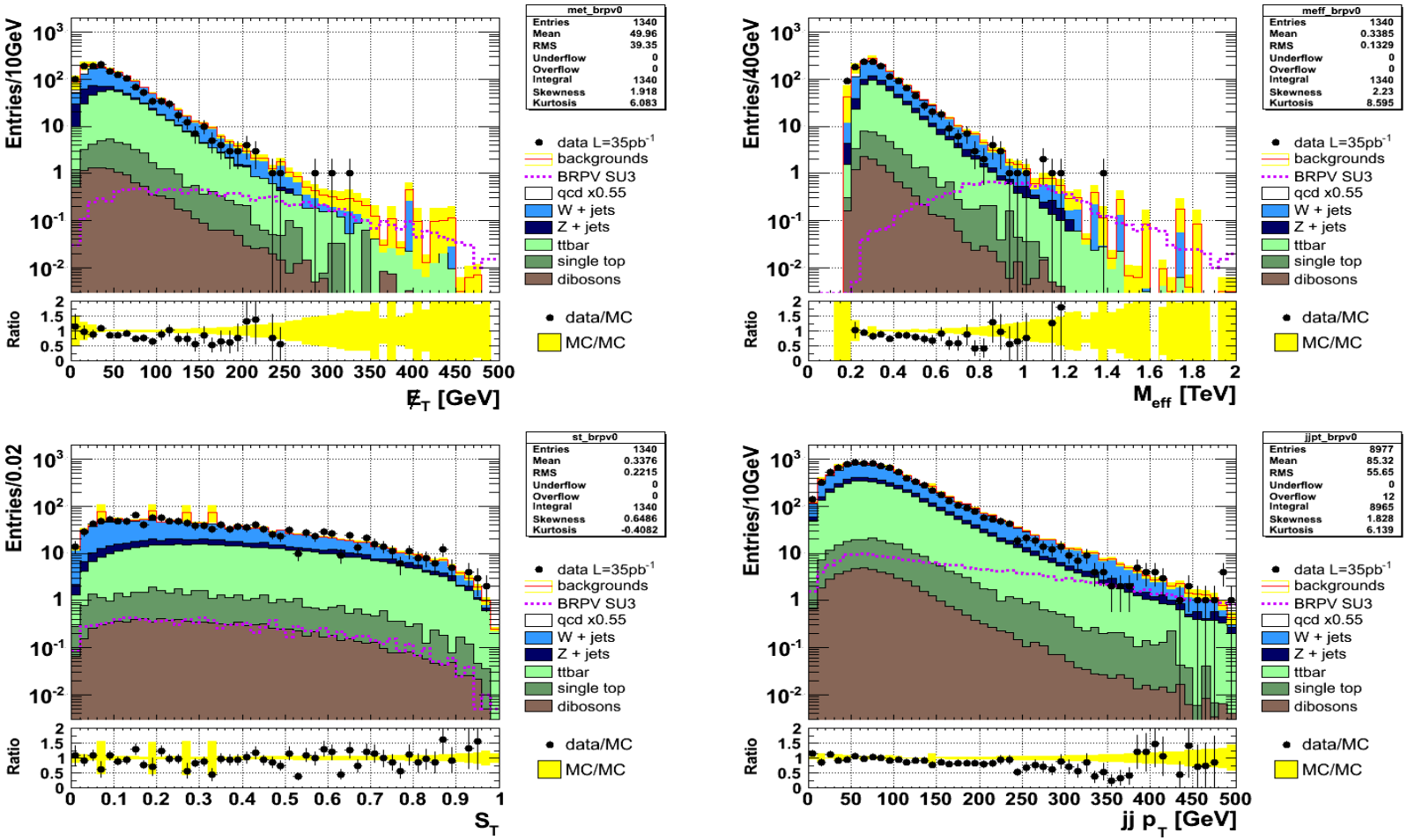

Figure: Left: $\not{E}_T$, S_T. Right: M_{eff}, p_T^{jj}. All at BRPV KS.

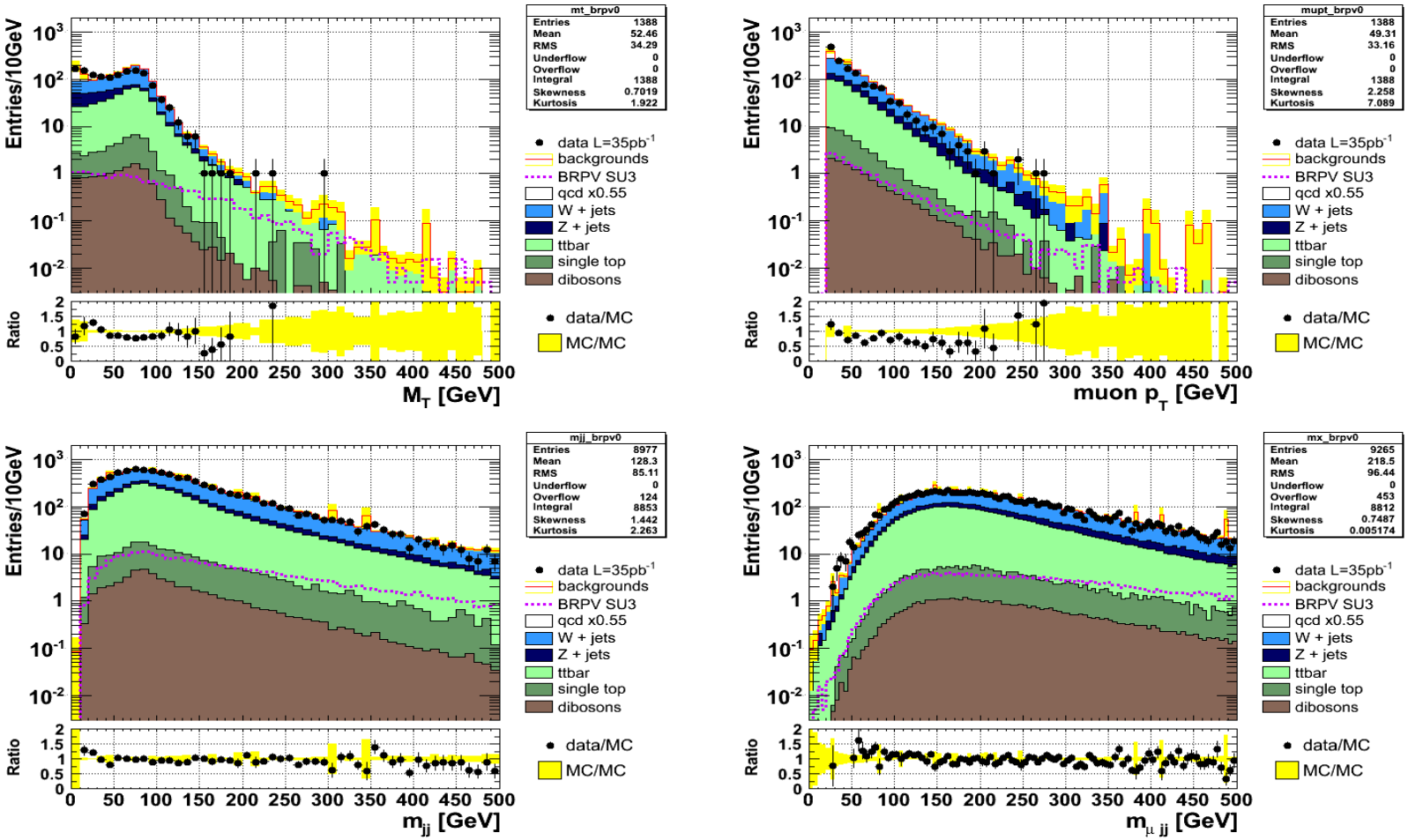

Figure: Left: M_T, m_{jj}. Right: p_T^{μ}, $m_{\mu jj}$. All at BRPV KS.

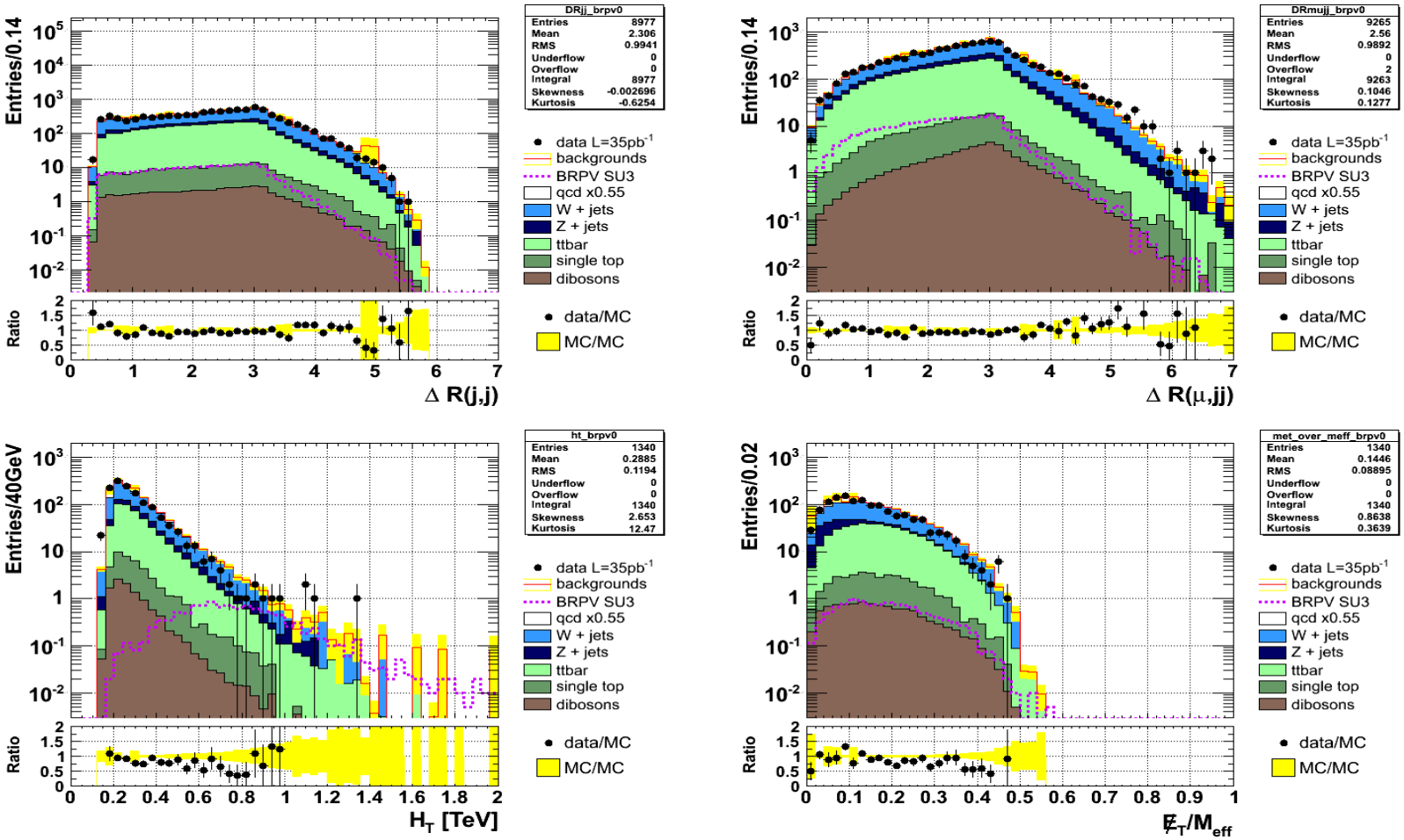

Figure: Left: $\Delta R(j,j)$, H_T. Right: $\Delta R(\mu,jj)$, $\not{E}_T/M_{\text{eff}}$, number of muons, number of reconstructed neutralinos. All at BRPV KS.

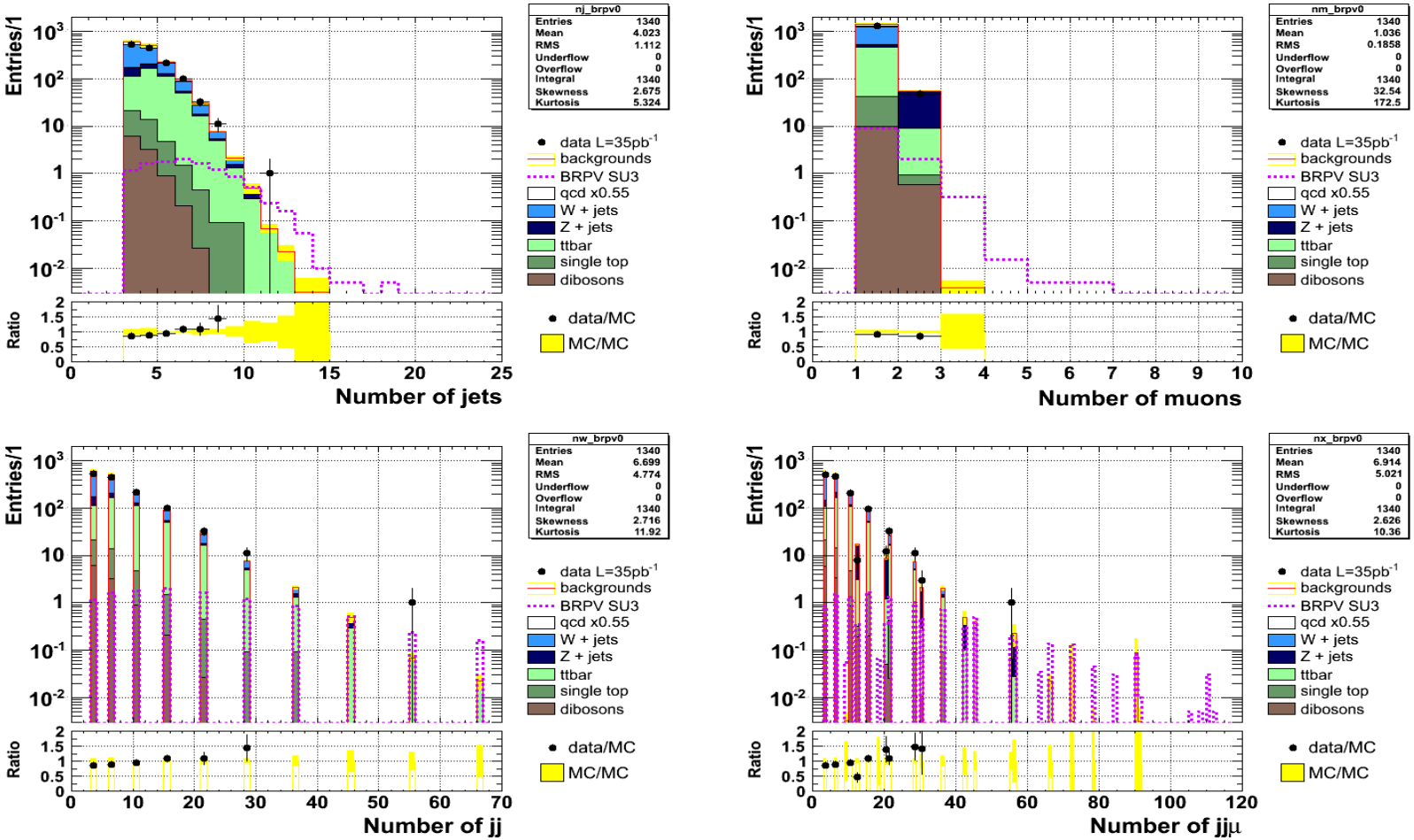

Figure: Left: number of jets, number of reconstructed W Bosons. Right: number of muons, number of reconstructed neutralinos. All at BRPV KS.

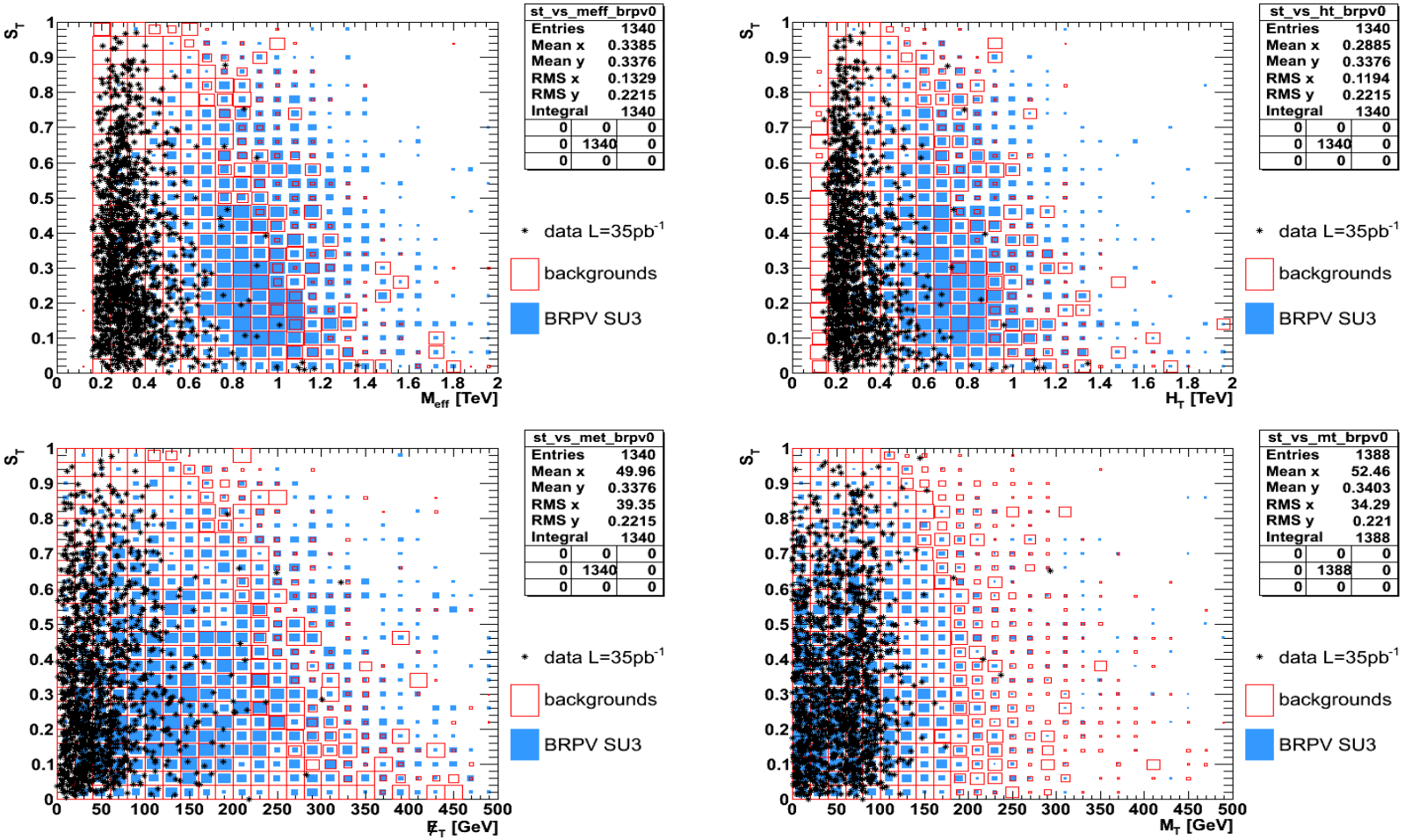

Figure: Left: S_T vs M_{eff}, S_T vs $\not{E}_T$. Right: S_T vs H_T, S_T vs M_T. All are at BRPV KS.

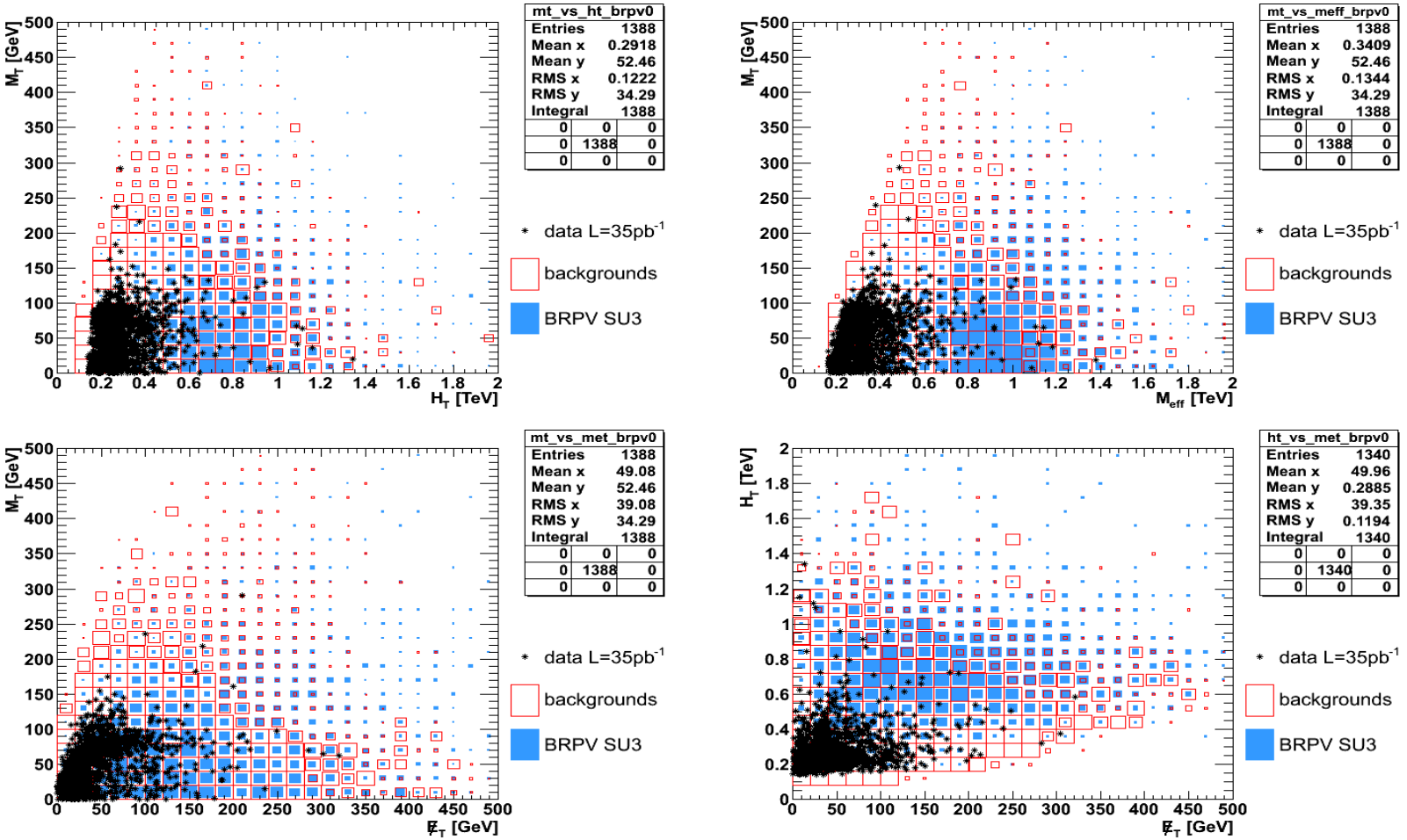

Figure: Left: M_T vs H_T, and M_T vs $\not{E}_T$. Right: M_T vs M_{eff}, and H_T vs $\not{E}_T$. All are at BRPV KS.

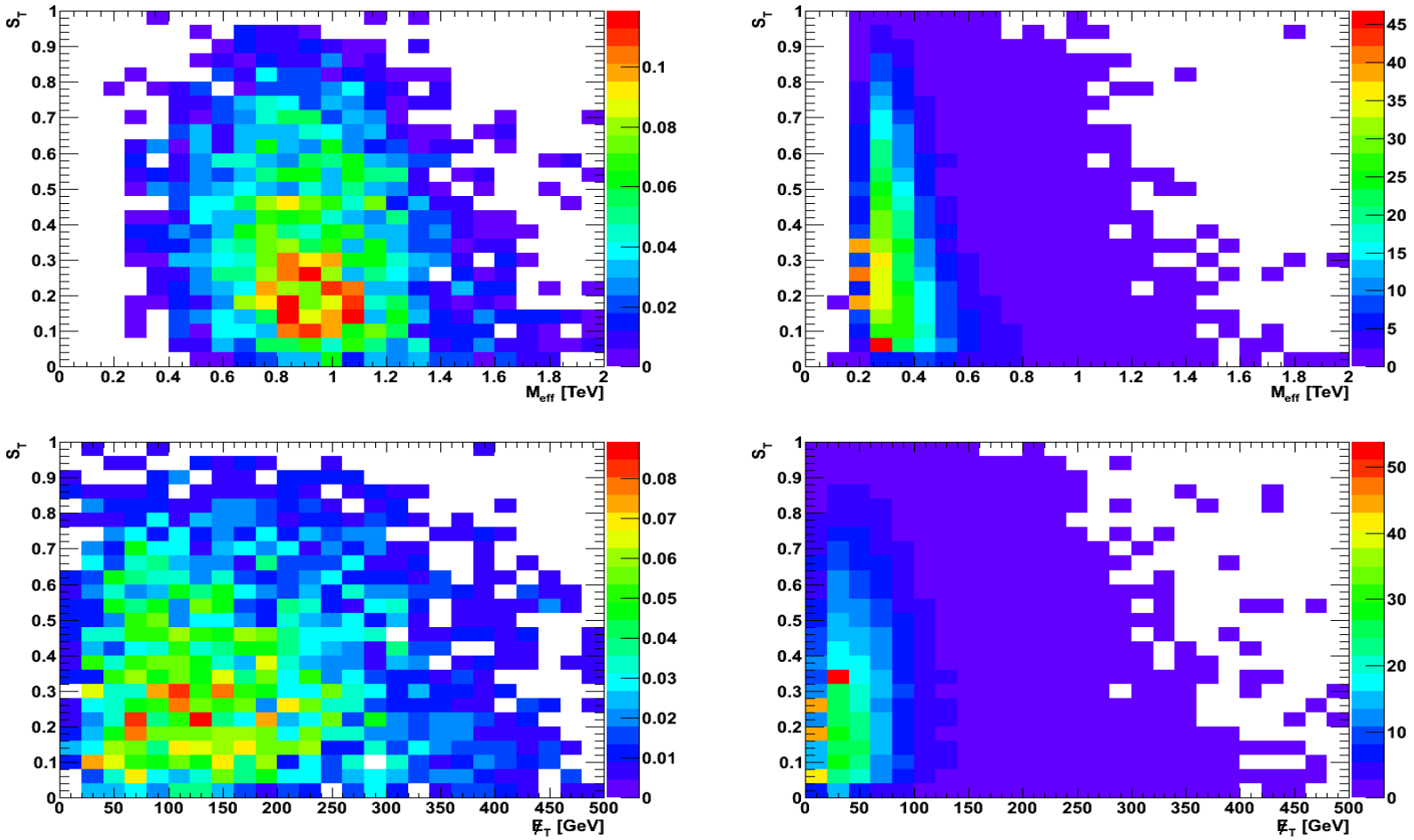

Figure: Bidimensional histograms, the left side plots are made using the BRPV SU3 signal sample, the right side plots are made using the sum of all MCB. The planes plotted are: S_T vs M_{eff} and S_T vs $\not{E}_T$. All are at BRPV KS.

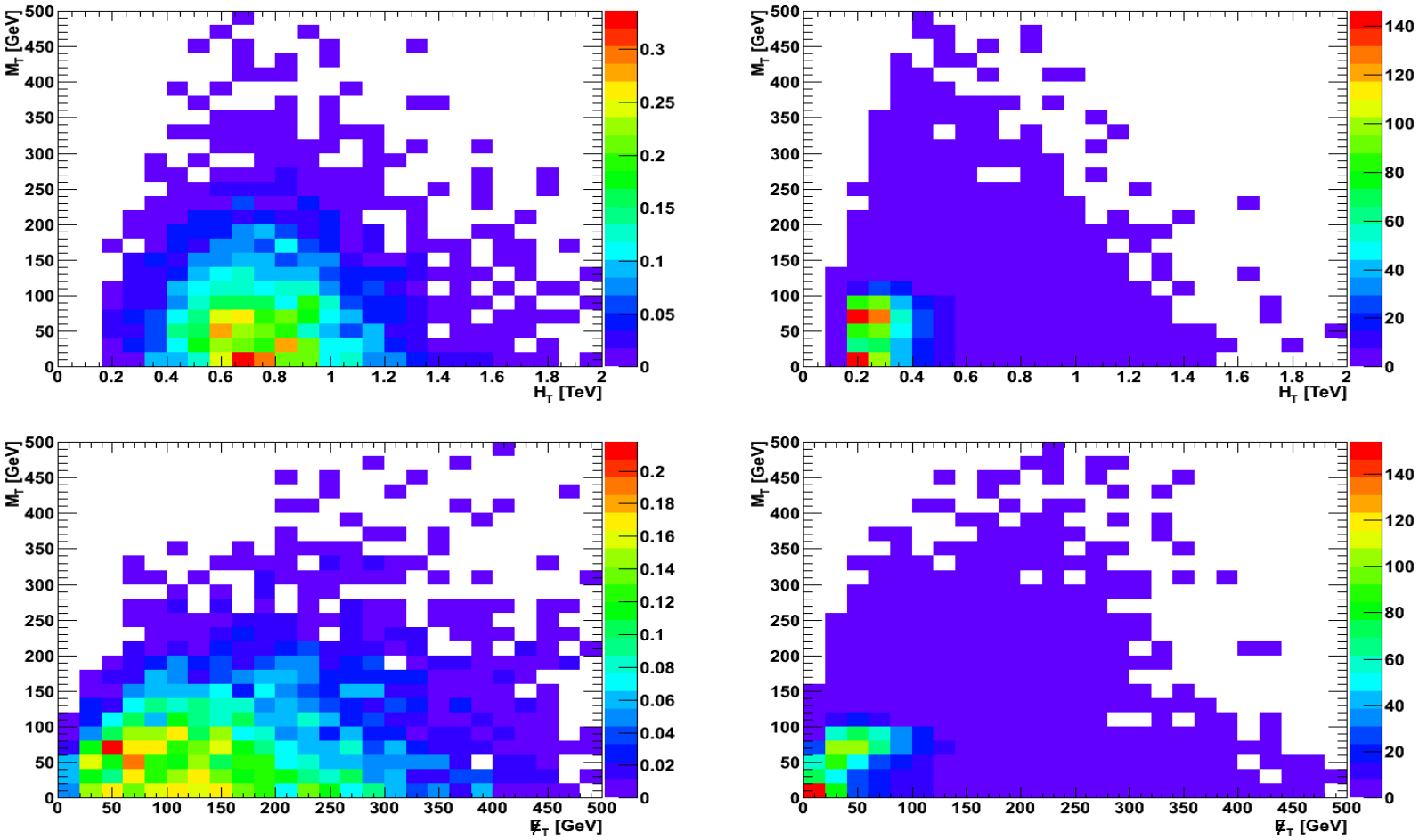

Figure: Bidimensional histograms, the left side plots are made using the BRPV SU3 signal sample, the right side plots are made using the sum of all MCB. The planes plotted are: M_T vs H_T, and M_T vs $\not{E}_T$. All are at BRPV KS.

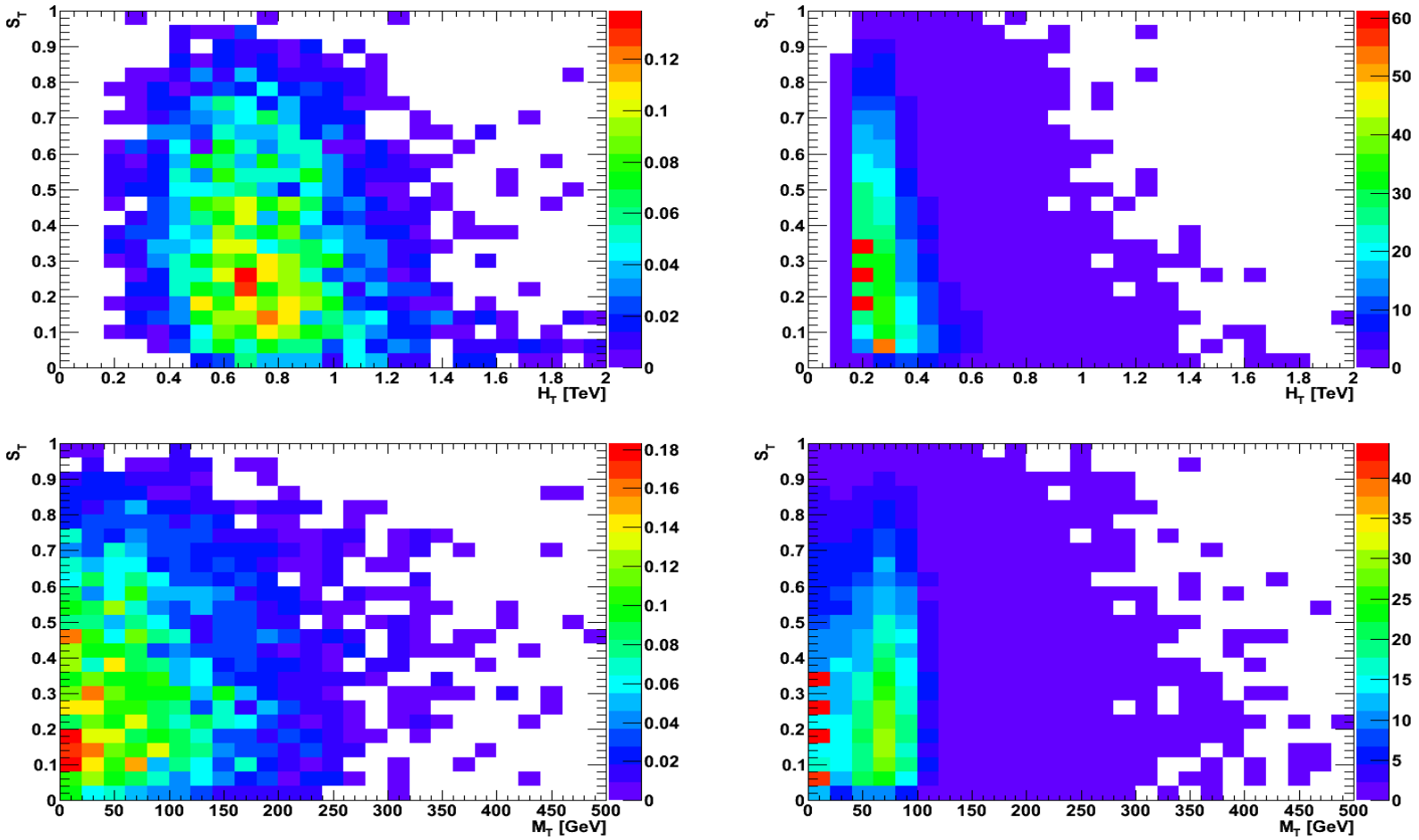

Figure: Bidimensional histograms, the left side plots are made using the BRPV SU3 signal sample, the right side plots are made using the sum of all MCB. The planes plotted are: S_T vs H_T and S_T vs M_T. All are at BRPV KS.

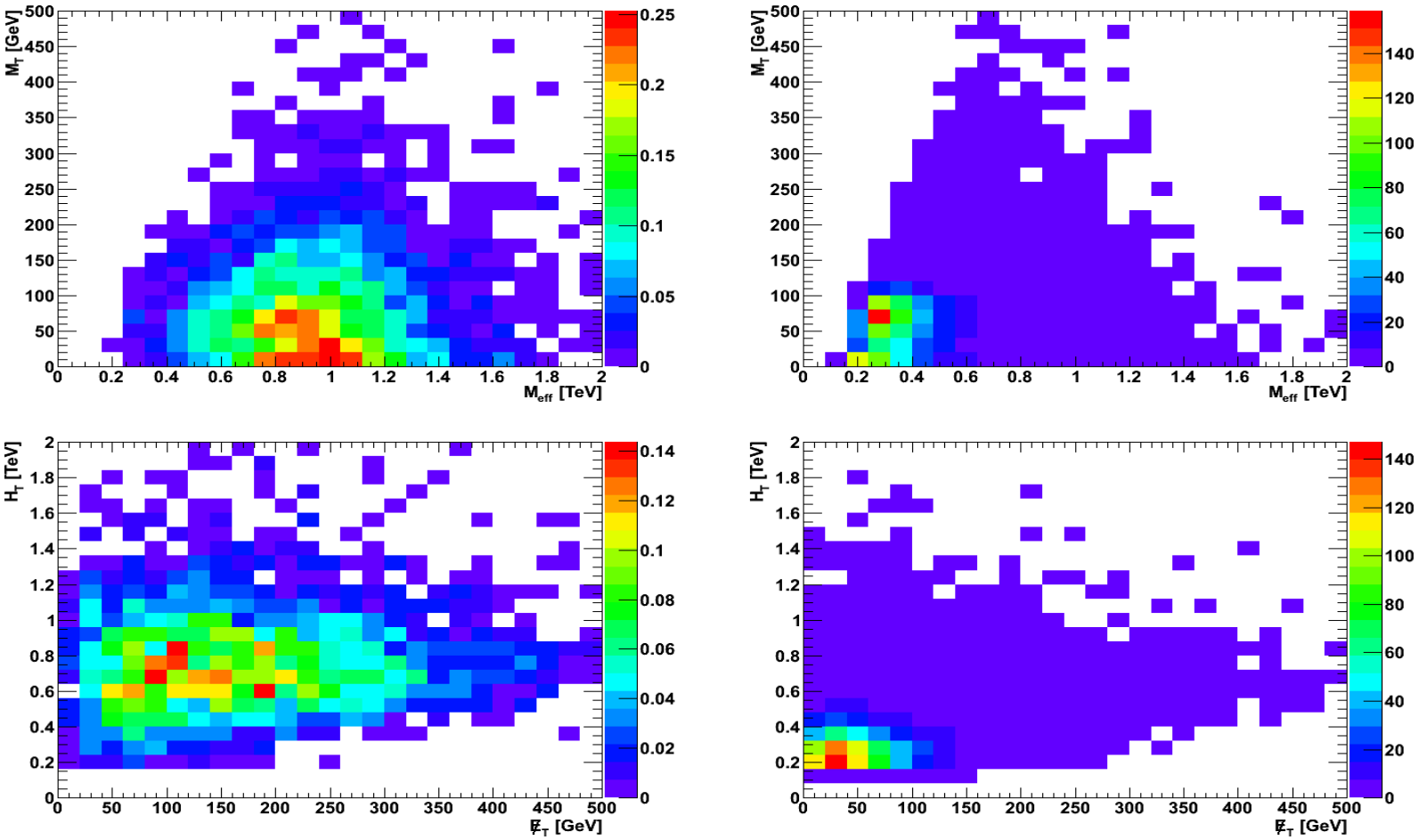

Figure: Bidimensional histograms, the left side plots are made using the BRPV SU3 signal sample, the right side plots are made using the sum of all MCB. The planes plotted are: M_T vs M_{eff} and H_T vs $\not{E}_T$. All are at BRPV KS.

Stats.

For purposes of discovering a new signal process, one defines the null hypothesis H_0 as describing only known processes, in this case, the sum of all MCB. This hypothesis to be tested against the alternative hypothesis H_1, which in this case, is the sum of all MCB plus the BRPV SU3 signal. When searching for a new phenomenon, one tries to reject H_0. If the p-value of H_0 is sufficiently low, then one is willing to accept that some alternative hypothesis is true. Often one converts the p-value into an equivalent significance Z, defined as Z standard deviation upward fluctuation of a Gaussian random variable would have an upper tail area equal to p, this is

$$Z = \Phi^{-1}(1 - p), \tag{73}$$

with Φ^{-1} the inverse of the cumulative distribution. The particle physics community has tended to regard rejection of H_0 with a significance of at least $Z = 5$, i.e. 5σ, as an appropiate level to constitute a discovery. This corresponds to $p = 2.87 \times 10^{-7}$. For purposes of excluding H_1, a threshold p-value of 0.05 (i.e. 95% of confidence level) is often used, which corresponds to $Z = 1.64$.

Likelihood function Considering an experiment where for each selected event one measures the values of certain kinematic variables, and thus the resulting data can be represented as one or more histograms. Suppose for each event in the signal sample one measures a variable x an uses these values to construct a histogram $\vec{n} = (n_1, ..., n_N)$. The expectation value of n_i can be written

$$E[n_i] = \lambda_{S_i} = \mu\, s_i + b_i, \tag{74}$$

where the mean number of entries in the ith bin fron signal and background are

$$s_i = s \int_{\text{bin } i} f_s(x, \vec{\theta_s}) dx, \tag{75}$$

$$b_i = b \int_{\text{bin } i} f_b(x, \vec{\theta_b}) dx. \tag{76}$$

Here μ determines the strenght of the signal process, with $\mu = 0$ corresponding to the H_0 and $\mu = 1$ being H_1. The functions $f_s(x, \vec{\theta_s})$ and $f_b(x, \vec{\theta_b})$ are the PDFs of the variable x for signal and background events, and $\vec{\theta_s}$ and $\vec{\theta_b}$ are parameters that characterize the shape of the PDFs. The quantities s and b are the total mean numbers of signal and backgrounds events, and the integrals 75 and 76 represent the probabilities for an event to be found in bin i. From now on we will use $\vec{\theta} = (\theta_s, \theta_b, b_{tot})$ to denote all of the nuisance parameters. The likelihood function is the product of Poisson probabilities for all bins n_i (for simplicity is assumed that the number of bins for the signal sample and the MC samples are the same)

$$L = \prod_{i}^{N} L_i \tag{77}$$

with

$$\begin{aligned} L_i(\vec{n}, \vec{\theta^0}|\mu, \vec{b}, \vec{\theta}) &= \frac{1}{n_{S_i}!}\lambda_{S_i}^{n_{S_i}} \exp\left(-\lambda_{S_i}\right) \\ &\cdot \prod_{I \in CR} \frac{1}{n_{I_i}!}\lambda_{I_i}^{n_{I_i}} \exp\left(-\lambda_{I_i}\right) \\ &\cdot P_{\text{syst}}(\vec{\theta^{0,i}}, \vec{\theta_i}), \end{aligned} \tag{78}$$

also is very useful the unbinned likelihood function, and is the last equation 78 but dropping the subindex i, i.e.

$$\begin{aligned} L(\vec{n}, \vec{\theta^0}|\mu, \vec{b}, \vec{\theta}) &= \frac{1}{n_S!}\lambda_S^{n_S} \exp\left(-\lambda_S\right) \\ &\cdot \prod_{I \in CR} \frac{1}{n_I!}\lambda_I^{n_I} \exp\left(-\lambda_I\right) \\ &\cdot P_{\text{syst}}(\vec{\theta^0}, \vec{\theta}), \end{aligned} \tag{79}$$

the unbinned likelihood function, is preferred since binning can only result in a loss of information, and hence larger statistical errors for the parameter estimates.

In equation 79, I run over CRs, and can take values Q, T, V that yields for qcd, top, W/Z plus jets, respectively; n_S is the number of observed events in the signal region, n_I is the number of observed events in the I-th control region, $\vec{\theta_0}$ are the nuisance parameters known a priori such as the cross section. The expected value of events λ in the signal region and in the control regions depends on the strength parameter μ ($\mu \geq 0$ gives collider physics, negative values of μ are present in neutrino physics), the nuisance parameters $\vec{b}$ and $\vec{\theta}$ via

$$\lambda_S(\mu, \vec{b}, \vec{\theta}) = \mu \cdot c_S^s(\vec{\theta}) \cdot s + \sum_j c_S^j(\vec{\theta}) \cdot b^j \tag{80}$$

$$\lambda_I(\mu, \vec{b}, \vec{\theta}) = \mu \cdot c_I^s(\vec{\theta}) \cdot s + \sum_j c_I^j(\vec{\theta}) \cdot b^j \tag{81}$$

where lower indices indicate the control region, upper indices indicate the control sample (or the process). The variables s and b^j are the total number of observed events of kind signal and j-th control sample respectively. Analogously j can take values: q, t, v. The transfer functions c come given by

$$c_I^j = \frac{\text{Number of events of kind j on the contol region I}}{\text{Number of events of kind j on the contol region J}} \times (1 + \vec{\Delta}_I^j \cdot \vec{\theta}) \tag{82}$$

with $\vec{\Delta}_I^j$ dealing with the uncertainties.

Equations 80 and 81 can be rewritten as a matrix equation like

$$\begin{pmatrix} \lambda_S \\ \lambda_Q \\ \lambda_T \\ \lambda_V \end{pmatrix} = \begin{pmatrix} \mu c_S^s & c_S^q & c_S^t & c_S^v \\ \mu c_Q^s & c_Q^q & c_Q^t & c_Q^v \\ \mu c_T^s & c_T^q & c_T^t & c_T^v \\ \mu c_V^s & c_V^q & c_V^t & c_V^v \end{pmatrix} \begin{pmatrix} s \\ b^q \\ b^t \\ b^v \end{pmatrix}, \tag{83}$$

where the sum of each column represents the acceptance of a specific process on all the control regions.

Statistic Test $\Lambda_\mu = -2 \ln l(\mu)$ The profile likelihood ratio $l(\mu)$ is defined as:

$$l(\mu) = \begin{cases} \frac{L(\vec{n},\vec{\theta}^0|\mu,\hat{\hat{\vec{b}}},\hat{\hat{\vec{\theta}}})}{L(\vec{n},\vec{\theta}^0|\hat{\mu},\hat{\vec{b}},\hat{\vec{\theta}})} & \hat{\mu} \geq 0, \\ \frac{L(\vec{n},\vec{\theta}^0|\mu,\hat{\hat{\vec{b}}},\hat{\hat{\vec{\theta}}})}{L(\vec{n},\vec{\theta}^0|0,\hat{\hat{\vec{b}}}(0),\hat{\hat{\vec{\theta}}}(0))} & \hat{\mu} < 0, \end{cases} \tag{84}$$

and the statistic test is:

$$\Lambda_\mu = -2 \ln l(\mu), \tag{85}$$

where $\hat{\hat{\vec{\theta}}}$, $\hat{\hat{\vec{b}}}$ [4] are the values of $\vec{\theta}(\mu)$ and $\vec{b}(\mu)$ that maximizes L (the conditional maximum-likelihood ML) for a given μ. The denominator is the (unconditional) likelihood function, where $\hat{\mu}, \hat{\vec{b}}$ and $\hat{\vec{\theta}}$ are their ML estimators.
p-value: The level of disagreement is parametrize by the p-value:

$$p_\mu = \int_{\Lambda_{\mu,obs}}^{\infty} f(\Lambda_\mu|\mu) d\Lambda_\mu, \tag{86}$$

where f is the PDF of the statistic Λ_μ. The PDF f is constructed using Montecarlo toy experiments by varying μ.

[4] Sometimes this value is hidden in $\vec{\theta}$, but in this work $\vec{\theta}$ is left to represent the uncertainties and another nuisance parameters.

Test statistic q_0 for a discovery:

$$q_0 = \begin{cases} -2 \ln l(0) & \hat{\mu} \geq 0, \\ 0 & \hat{\mu} < 0, \end{cases} \tag{87}$$

$$p_0 = \int_{q_0,obs}^{\infty} f(q_0|0) dq_0. \tag{88}$$

If the data fluctuate and one finds fewer events than even predicted by background process alone, then $\hat{\mu} < 0$ and one has $q_0 = 0$ (agreement with the background only hypothesis, *no discovery*).
If one finds more events than the expected backgrounds b_l^j i.e. for increasing $\hat{\mu}$ increasingly large values of q_0 are found. This corresponds to an increasing level of incompatibility between the data and the $\mu = 0$ hypothesis, *discovery*.
Test statistic q_μ for upper limits.:

$$q_\mu = \begin{cases} -2 \ln l(\mu) & \hat{\mu} \leq \mu, \\ 0 & \hat{\mu} > \mu, \end{cases} \tag{89}$$

$$p_\mu = \int_{q_\mu,obs}^{\infty} f(q_\mu|\mu) dq_\mu. \tag{90}$$

The reason for setting $q_\mu = 0$ for $\hat{\mu} > \mu$ is that when setting and upper limit, one would not regard data with $\hat{\mu} > \mu$ as representing compatibility with μ than the data obtained, and therefore this is not taken as part of the rejection region of the test. From the definition of the test statistic one sees that higher values of q_μ represent greater incompatibility between the data and the hypothesis value of μ.

SR and CRs

A CR of some background i, is the specific zone in the variables space per event, where the probability distribution function (PDF) of the variables (histograms) of the $i-$th background, dominates over the variables of the another backgrounds. The most relevant MCB samples for the final states of this work are decaying vector boson plus jets ($V+$jets, the union of $Z+$jets and $W+$jets), $t\bar{t}$ and QCD. The $Z+$jets and $W+$jets MCB were unified because at BRPV KS there was not possible to separate them by using cuts on kinematic variables. The control regions CR are defined in order to take control on the behavior of the relevant MCB.

QCD Control Region: This CR is defined by demanding:

1. BRPV KS,
2. $\not\!\!E_T < 40$ GeV, and
3. $M_T < 40$ GeV

V+jets Control Region: This CR is defined by demanding:

1. BRPV KS,
2. 30 GeV $\leq \not{E}_T <$ 80 GeV,
3. 40 GeV $\leq M_T <$ 80 GeV, and
4. none b-jet in the first three leading jets of the event.

The last requirement is made demanding that all jets have a weight flavor less than 5.72.

$t\bar{t}$ Control Region: This CR is defined by demanding:

1. BRPV KS,
2. 30 GeV $\leq \not{E}_T <$ 80 GeV,
3. 40 GeV $\leq M_T <$ 80 GeV, and
4. the presence of at least one b-jet in the first leading jets of the event.

It is very interesting the little excess of data over the sum of MCB in the plot of the reconstructed invariant mass $m_{\mu jj}$, on the range between 90 GeV and 150 GeV, figure 22. In this plot, the signal BRPV SU3 does not explain the excess. If this excess would pass the statistical test for discovery (disagreement with the background only hypothesis), it would be an example of an *independent new physics model* of the signal tested.

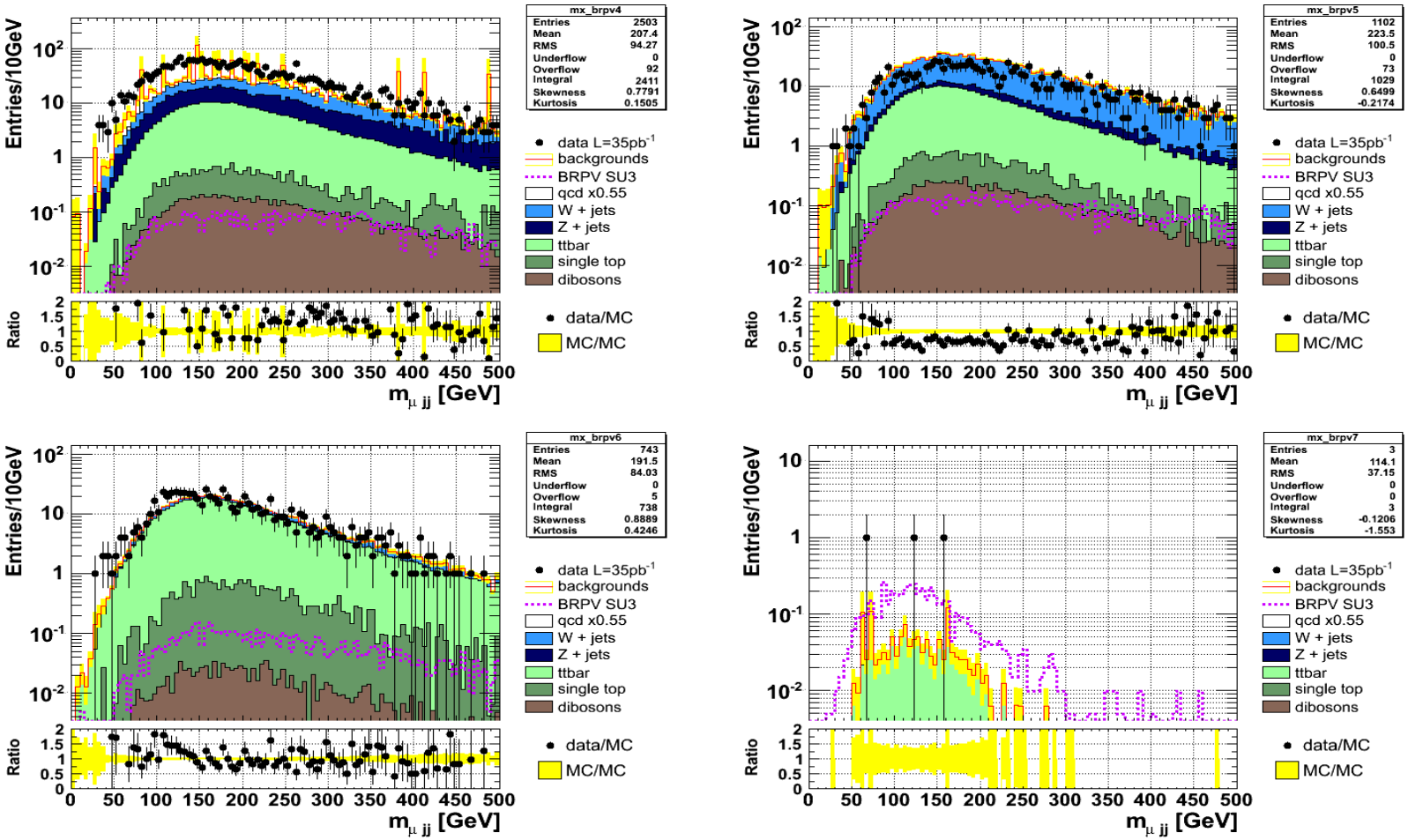

Figure: $m_{\mu jj}$ at different control regions. Left Top: QCD CR, Right Top: $V + jets$ CR, Left Bottom: $t\bar{t}$ CR, and Right Bottom: SR

Signal Region: This CR is defined by demanding:

1. BRPV KS,
2. cut on the S_T, M_{eff} plane:

$$\begin{cases} S_T \leq 0.125 & \text{if } M_{\text{eff}} > 0.8 \text{ TeV} \\ S_T > 1.0 - \dfrac{2.1875}{\text{TeV}} \cdot (M_{\text{eff}} - 0.4 \text{ TeV}) & \text{if } S_T > 0.125 \end{cases} \tag{91}$$

3. the mass of the jj pairs must stay in a window mass of width equal to 55 GeV and centered at the W Boson mass of 80.39 GeV,
4. cut on the transverse momentum of the jj pairs: $p_T > 20$ GeV,
5. cut on the angular distance between jets forming a jj: $\Delta R(j,j) < 2.9$,
6. cut on the angular distance between the jj pairs and the muon: $\Delta R(jj,\mu) < 1.1$, this cut is very important and provides very much for the gaussianity of the reconstructed neutralino mass for values greater than the simulated neutralino mass of 118 GeV.
7. again a cut on the transverse sphericity $S_T > 0.25$, this cut is made in order to remove the remaining of the Z+jets background,
8. $\not{E}_T > 130$ GeV, with this cut one can rule out the remaining of the W+jets background.

The cut in eq. 91, can be guessed for seeing the figure 18. The criteria to find this signal region SR was the ability to reconstruct the simulated neutralino invariant mass of the BRPV SU3 sample, and it can be seen in figures 23 and 24, each plot was made after each cut of the signal region definition. It is found that there are three ocurrences of reconstructed μjj objects, of which, two are not candidate to neutralino if we close the W boson mass window, i.e. to require reconstructed W boson more on-shell than before.

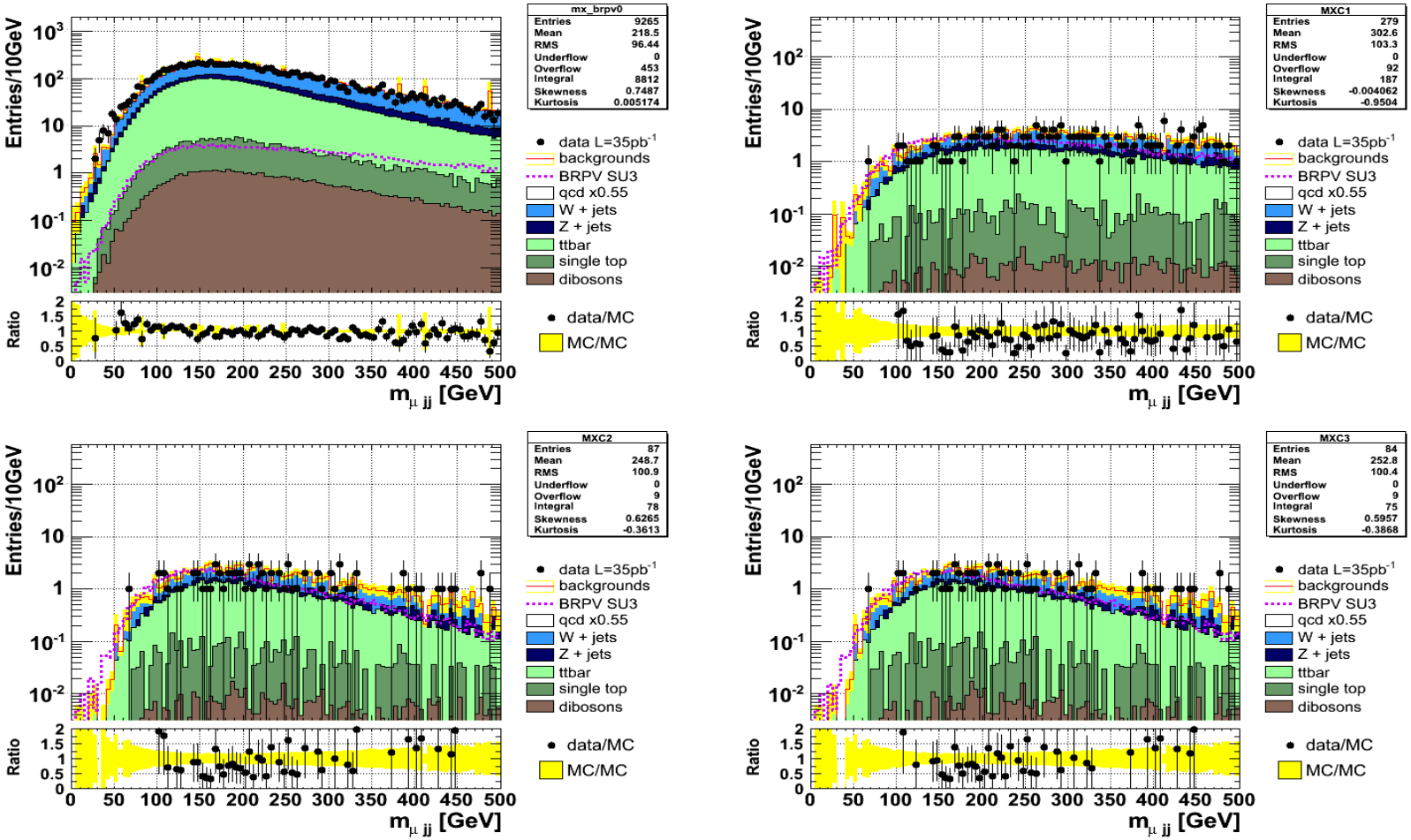

Figure: Reconstructed Neutralino that decays into a W Boson and a muon, the W Boson is assumed to decays to two jets. Every plot was made after each cut on the signal region definition. Reading order: from left to right.

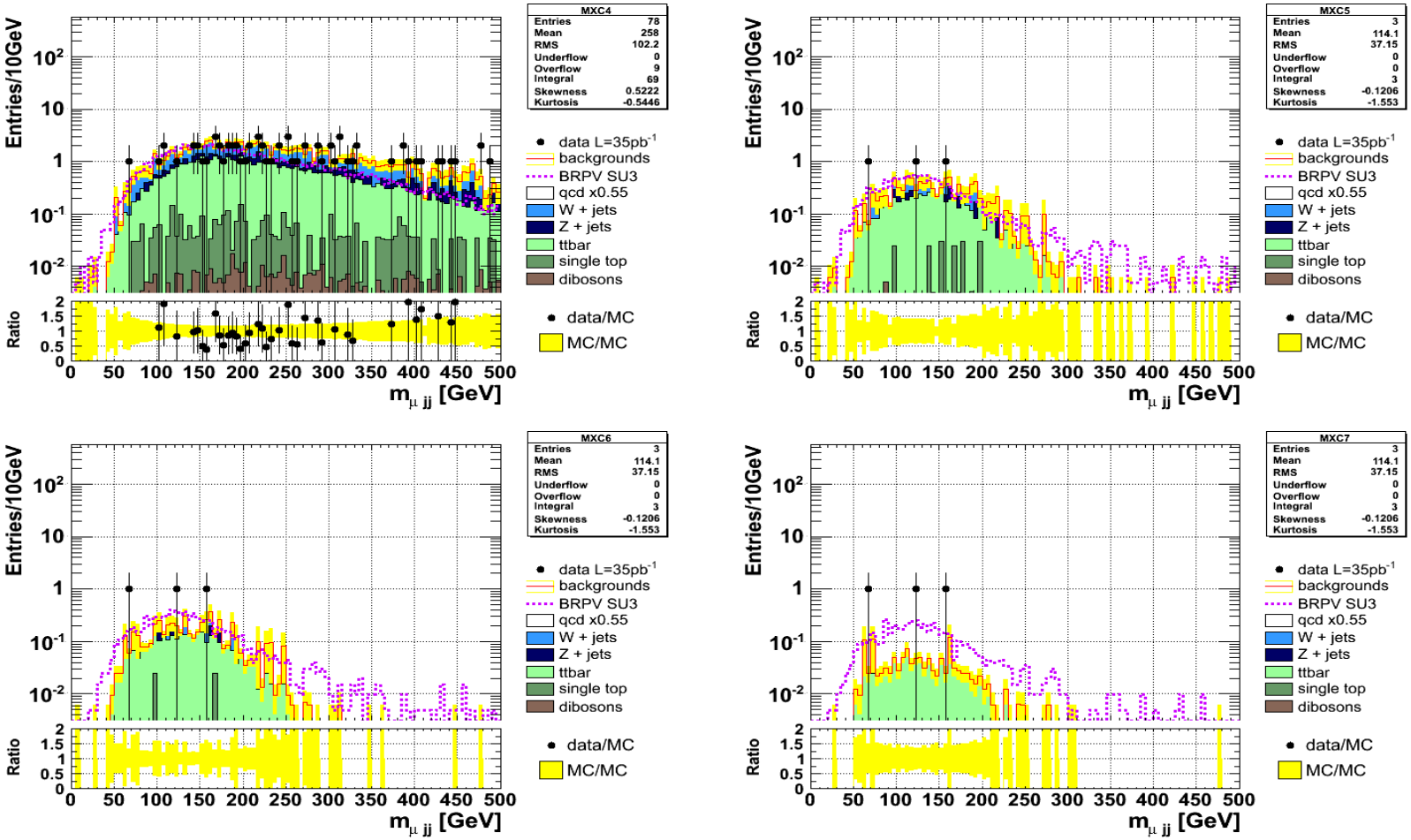

Figure: Reconstructed Neutralino that decays into a W Boson and a muon, the W Boson is assumed to decays to two jets. Every plot was made after each cut on the signal region definition. Reading order: from left to right.

The survival event for real data in the SR, corresponds to the event number 38'547,952, and belongs to the run number 167,776 of period I. This period was taken in November of 2010. This event has: $\not{E}_T = 246.8$ GeV, $\phi^{\not{E}_T} = -0.264$, $M_{\text{eff}} = 750.1$ GeV, Number of signal muons equals to one, Number of signal jets equals to eight from which one of them is a b-jet, Number of signal electrons equals to zero, $M_T = 99.72$ GeV, and the muon have: $E^{\mu} = 75.89$ GeV, $p_T^{\mu} = 46.26$ GeV, $\eta^{\mu} = -1.079$, $\phi^{\mu} = -1.235$ rad. Figure 25 shows the planes: ρz at the bottom, yx at top-right, and $\phi\eta$ at top-left. Outside the detector are the region of interest ROI for: the jets (gray), taus (gray), and muons (light red). While inside the detector are: jets (gray), tracks (cyan), one muon (red light), $\not{E}_T$ (dark red with arrow), and b-jet (blue).

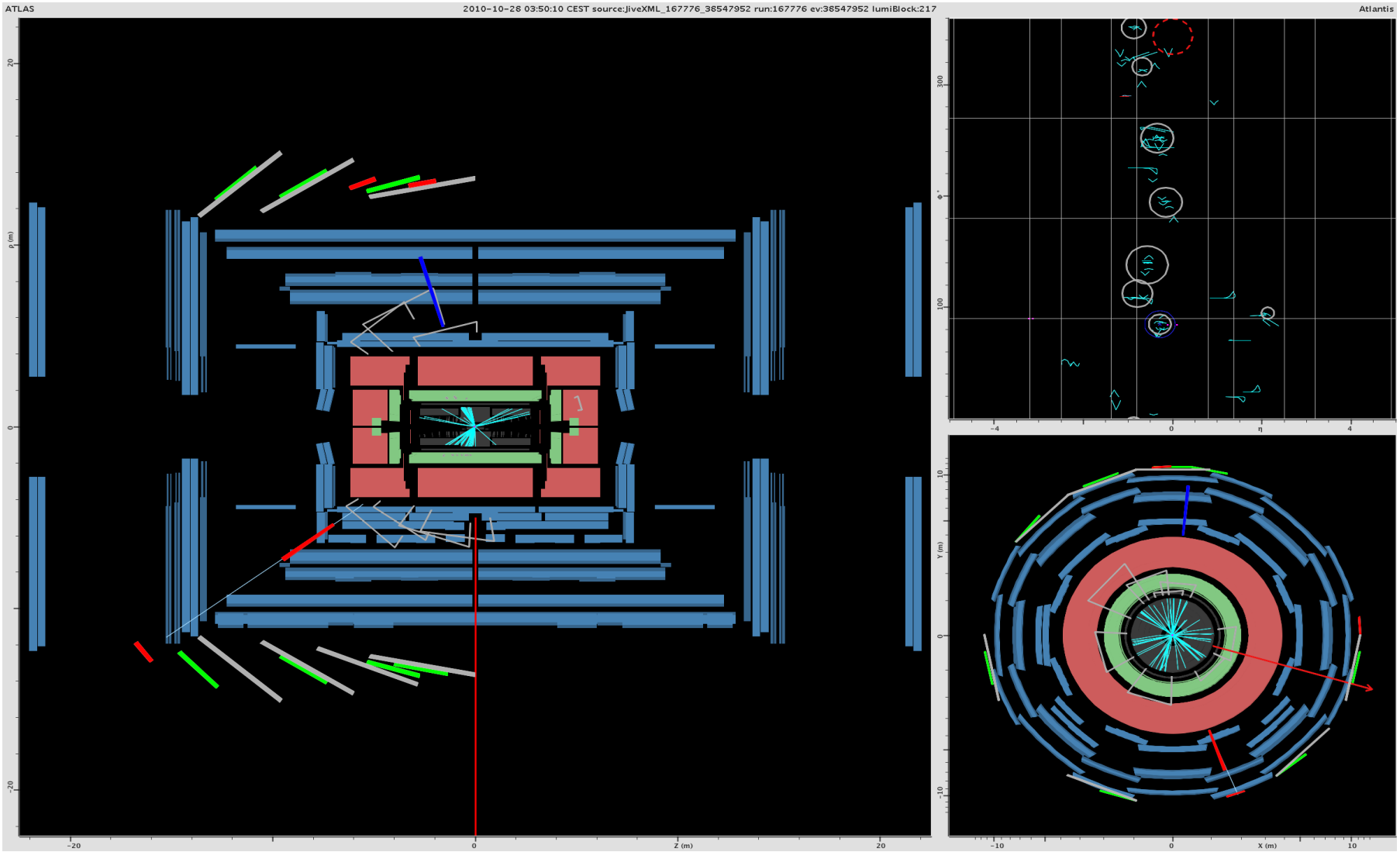

Figure: Event 38'547,952 from RunNumber 167,776 of period I. The plot was done with Atlantis by processing the information stored on an AOD, so the calorimeter cell deposits are not present here. Outside the detector are the region of interest ROI for: the jets (gray), taus (gray), and muons (light red). While inside the detector are: jets (gray), tracks (cyan), one muon (red light), $\not{E}_T$ (dark red with arrow), and b-jet (blue). Planes: ρz at bottom, yx top-right, $\phi\eta$ at top-left.

Final

CR \Sample	qcd	v+jets	$t\bar{t}$	brpv su3	data 2010
QCD	140.8	148.4	44.31	0.3363	395
V+JETS	1.275	199.6	37.32	0.4847	168
$T\bar{T}$	0.03269	13.7	75.33	0.3017	113
BRPV SU3	0	0.1879	0.6481	1.909	1

Table: Number of survivor events in the CRs.

$$\begin{pmatrix} \lambda_S \\ \lambda_Q \\ \lambda_T \\ \lambda_V \end{pmatrix} = \begin{pmatrix} \mu \cdot 1 & 0 & 0.008603478 & 0.002428357 \\ \mu \cdot 0.176165532 & 1 & 0.588211868 & 0.743486974 \\ \mu \cdot 0.158040859 & 0.000232173 & 1 & 0.068637275 \\ \mu \cdot 0.253902567 & 0.009055398 & 0.495420151 & 1 \end{pmatrix} \begin{pmatrix} 1.909 \\ 140.8 \\ 75.33 \\ 199.6 \end{pmatrix} . \quad (92)$$

Unfortunately the uncertainty of the cross section calculation for the BRPV SU3 sample was not properly calculated at the time of writing this work. The systematic uncertainties for the control regions, Jet/Muon/Electron resolution scales (JERS,MERS,EERS) were not taking into account too. So the long likelihood profile ratio method could not be entirely applied here. Besides that, from figure 24 can be seen, that there was not enough integrated luminosity to approve the BRPV SU3 hypothesis, because we could not kill the sum of all MCB without kill the BRPV SU3 signal (We could not observed at least one bin with frequency greater than 1, for the BRPV SU3 signal in the SR). For the same reasons the LLR method was not applied on the mass histogram of the reconstructed μjj object in thre $t\bar{t}$ CR, but certainly this behaviour (possible independent new physics model of the signal tested) should be investigated in more detail by adding the 2011 data; if the same behaviour is keeped, it will be necessary to propose a new theoretical signal that explains this excess.

Summary

In this work an early susy search at $\sqrt{s} = 7$ TeV at integrated luminosity of 35 pb^{-1} with the ATLAS detector was made. To this pourpose a specific channel was stablished: $\tilde{\chi}_1^0 \to W\mu \to jj\mu$, the search started by picking out the release 6.20 susy D3PD samples, data, Montecarlo, and signal, afther this, defining all the physical objects according to the CERN susy working group standards, this rules were appearing and changing along the 2010 year, the physical objects were: electrons, muons, jets and missing energy transverse, with this, some kinematic variables were constructed: transverse sphericity, transverse mass, scalar mass, effective mass. Then the reconstructed W boson was made by summing the four-momentum of different jets in the events and then the four-momentum of the reconstructed W boson were summed with the four-momentum of the muons in order to find the reconstructed neutralino. At this point a lot of variables in this specific channel were ready to start the physics analysis. The first thing was to find a kinematic selection that was called BRPV KS and then calibrate the data with the summ of all Montecarlo backgrounds by using the most important variable $\not{E}_T$ in its validity range [0,200] GeV, to this pourpose an scale of 0.55 on the QCD MCB was applied. Here the road towards to apply the profile LLR was started, firstable by defining good control regions for the most relevant Montecarlo backgrounds, and finding a signal region. After that the contamination coefficients were calculated without using the systematic uncertainties, by using the table 12, then the matrix 92 was constructed. Unfortunately the road was truncated here, but by seeing figure 24 the discovery hypothesis can be discarded.

Conclusions

The BRPV SU3 mSUGRA point could not reproduce the real data observed for the 2010 year at the ATLAS detector with 35 pb^{-1}.
In the way to apply the LLR, we could obeserve a little excess of data over the sum of the MCB. This excess can not be explained with the BRPV SU3 point. This have to be research in a near future. It is necessary to make a grid of mSUGRA points for BRPV susy, i.e. varying the m_0, and $m_{1/2}$ parameters. A solid base for the 2011 data analysis with ATLAS for any kind of channel was stablished, this because the object definitions fullfil the high standards required by the ATLAS community, and because the decision to keep running at $\sqrt{s} = 7$ TeV will allow to use either these objects definitions or these with a few little changes. For future works a deeper inside on the statistical techniques needs to be masterized, among them are: profile LLR, Bayesian approaches, neural networks, and boosted decision trees (BDT)
Classification and Regression Trees. Chapman & Hall 1984,
Experiments with a New Boosting Algorithm. 13th Conference on Machine Learning 1996.
Being the last one, the technique used to guess the best cuts given an input requirement. A modular, structurated, robust, and scalable software to research HEP at ATLAS was created and released with GNU/GPL v.3 license
http://www.gnu.org/copyleft/gpl.html,
this project was placed on
http://code.google.com/p/muon-plus-2-jets-channel/,
and anybody can browse it, use it, and to learn from it. This was the first time that the HEPPUC at Pontificia Universidad Católica de Chile do an study on CERN real data, so this work represents a tremendous technological improve for our region.